

# Scale-Dependent Multifractality in Bitcoin Realised Volatility: Implications for Rough Volatility Modelling

Milan Pontiggia

Master's Student, MAGEFI – Magistère in International Economics and Finance University of Bordeaux, France

September 23, 2025

## Abstract

We assess the applicability of rough volatility models to Bitcoin realised volatility using the normalised  $p$ -variation framework of Cont and Das (2024). Applying this model-free estimator to high-frequency Bitcoin data from 2017 to 2024 across multiple sampling resolutions, we find that the normalised statistic remains strictly negative throughout, precluding the estimation of a valid roughness index. Stationarity tests and robustness checks reveal no significant evidence of non-stationarity or structural breaks as explanatory factors. Instead, convergent evidence from three complementary diagnostics, namely Multifractal Detrended Fluctuation Analysis, log-log moment scaling, and wavelet leaders, reveals a multifractal structure in Bitcoin volatility. This scale-dependent behaviour violates the homogeneity assumptions underlying rough volatility estimation and accounts for the estimator's systematic failure. These findings suggest that while rough volatility models perform well in traditional markets, they are structurally misaligned with the empirical features of Bitcoin volatility.

# Contents

<b>1</b>	<b>Introduction</b>	<b>2</b>
1.1	Background and Motivation . . . . .	2
1.2	Research Gap . . . . .	3
1.3	Research Question and Empirical Puzzle . . . . .	3
1.4	Hypotheses . . . . .	4
1.5	Contributions . . . . .	4
<b>2</b>	<b>Literature Review</b>	<b>5</b>
2.1	Rough Volatility and the Hurst Paradigm . . . . .	5
2.2	The Cont–Das Normalised $p$ -Variation Estimator . . . . .	5
2.3	Multifractality in Financial Time Series . . . . .	6
<b>3</b>	<b>Data and Methodology</b>	<b>7</b>
3.1	Mathematical Framework . . . . .	7
3.2	Data Description and Preprocessing . . . . .	8
3.3	Realised Volatility Construction . . . . .	11
3.4	Diagnostic Exploration: Roughness vs $K$ . . . . .	12
3.5	Final Estimation Setup . . . . .	15
3.6	Diagnostic Tests . . . . .	15
3.6.1	Non-Stationarity Diagnostics . . . . .	15
3.6.2	Multifractality Diagnostics . . . . .	16
<b>4</b>	<b>Empirical Results</b>	<b>17</b>
4.1	Main Result: Roughness Estimation behaviour . . . . .	17
4.2	Stationarity and Window Stability . . . . .	19
4.3	Evidence of Multifractality . . . . .	19
4.4	Hypothesis Evaluation . . . . .	20
<b>5</b>	<b>Discussion</b>	<b>21</b>
5.1	Structural Interpretation . . . . .	21
5.2	Implications for Modelling . . . . .	22
5.3	Practical Consequences . . . . .	22
5.4	Limitations and Future Work . . . . .	23
<b>6</b>	<b>Conclusion</b>	<b>24</b>
	<b>Appendix A: Supplementary Tables</b>	<b>25</b>
	<b>Appendix B: Supplementary Figures</b>	<b>36</b>
	<b>Appendix C: Code and Data Availability</b>	<b>40</b>

# 1 Introduction

## 1.1 Background and Motivation

The rough volatility framework has emerged as a prominent approach for modelling the fine-scale dynamics of financial market volatility. This development is grounded in empirical findings that indicate that realised volatility paths possess low Hölder regularity, which implies irregularity in their sample paths at high frequencies. Rough stochastic volatility models have been shown to replicate empirical features commonly observed in financial markets, including volatility clustering, short-term persistence, and the skew and term structure of implied volatility surfaces in equity and index markets Gatheral et al. (2018); Fukasawa et al. (2022). These observations have motivated attempts to extend the applicability of rough volatility models to nontraditional asset classes.

However, the extent to which this framework generalises to structurally distinct markets remains an open empirical question. Bitcoin, the most liquid and actively traded cryptocurrency, offers a particularly informative out-of-sample test. Unlike traditional equity or FX markets, Bitcoin exhibits fragmented liquidity across exchanges Makarov and Schoar (2020), frequent discontinuities due to jumps Lahmiri and Bekiros (2020), regime-switching volatility Caporale and Zekokh (2021), and an evolving market microstructure shaped by protocol changes and shifting incentives Easley et al. (2019). This motivates a closer empirical examination of whether rough volatility assumptions hold in such a market.

In this context, the term *roughness* refers to the local irregularity of the volatility path, quantified in terms of its Hölder regularity. A process is said to be *rough* if its sample paths exhibit lower regularity than the sample paths of Brownian motion. This notion of roughness is mathematically formalised via the concept of a *roughness index*, the reciprocal of the smallest  $p \geq 1$  such that the process admits finite  $p$ -variation along a refining partition sequence. In rough volatility models,  $H$  captures the scaling properties of volatility at infinitesimal time scales, and accurately estimating it is essential for determining whether volatility exhibits statistically significant roughness.

Prior applications of rough volatility methodologies to Bitcoin have predominantly employed parametric inference techniques or heuristic scaling diagnostics, often without systematically assessing assumptions of homogeneous Hölder continuity Bianchi et al. (2022). Empirical studies on cryptocurrencies more broadly, including Liu and Tsyvinski (2021), have concentrated on asset pricing and factor models, without directly addressing the scaling properties of volatility. The normalised  $p$ -variation estimator recently introduced by Cont and Das (2024) provides a model-free approach to estimating the pathwise roughness of volatility signals. This estimator offers two notable advantages over traditional methods based on log-volatility increments or variogram regressions: (i) it exhibits improved asymptotic properties under general conditions, and (ii) it is less sensitive to microstructure noise and finite-sample distortions. These properties make it especially suitable for high-frequency volatility data in contexts like cryptocurrency markets, where noise and irregular sampling are common.

This study builds on the normalised  $p$ -variation estimator introduced by Cont and Das (2024) to perform a systematic evaluation of the roughness of Bitcoin realised volatility across a range of sampling frequencies and time horizons. This analysis examines the applicability of rough volatility models to Bitcoin and contributes to a deeper understanding of the structural features that differentiate cryptocurrency volatility dynamics.

## 1.2 Research Gap

While the rough volatility literature has made significant progress in recent years, its empirical evidence is drawn primarily from equity and index markets. In these settings, various empirical methodologies, including parametric estimation and  $p$ -variation diagnostics, have provided evidence for the existence of a global scaling regime consistent with rough stochastic volatility models. However, the applicability of such models to structurally distinct markets such as cryptocurrencies remains largely unexplored.

Bitcoin’s volatility displays structural features such as multiscale clustering, episodic jumps, and irregular liquidity that differ markedly from the conditions under which rough volatility models have been validated. For instance, Bianchi et al. (2022) report low Hurst exponents for Bitcoin by fitting rough stochastic volatility models and performing scaling regressions on realised volatility. However, their approach implicitly assumes a global scaling regime and stationarity, without subjecting these conditions to empirical verification. These assumptions are critical, and their violation under multifractal dynamics or structural irregularities undermines the reliability of such roughness estimates. Crucially, no prior work has systematically examined whether Bitcoin realised volatility meets the homogeneity and stationarity conditions required for consistent estimation via the normalised  $p$ -variation method.

Moreover, recent research indicates that the observed roughness of realised volatility may arise from estimation error rather than genuine features of the spot volatility process Cont and Das (2024); Rogers (2019). In the case of Bitcoin, where multifractality and non-stationarity are theoretically plausible features, this raises serious doubts about the robustness and interpretive value of roughness estimates.

To our knowledge, no prior empirical study has systematically applied the  $p$ -variation diagnostic to Bitcoin realised volatility, nor has tested its structural compatibility with the assumptions underlying rough volatility models. It remains empirically unestablished whether Bitcoin volatility admits a well-defined roughness exponent. This study addresses this gap by applying the model-free normalised  $p$ -variation estimator alongside complementary diagnostic methods.

## 1.3 Research Question and Empirical Puzzle

This study tests whether Bitcoin realised volatility satisfies the homogeneous scaling assumptions necessary for consistent roughness estimation under the rough volatility paradigm.

We investigate this question by applying the normalised  $p$ -variation methodology of Cont and Das (2024) to Bitcoin realised volatility across multiple years and sampling frequencies. Preliminary results indicate that, in contrast to equity and foreign exchange markets, Bitcoin volatility does not appear to admit a well-defined roughness index. This stands in contrast to prior findings for equity and foreign exchange markets, where roughness estimates have exhibited consistent behaviour and robust interpretability.

This empirical anomaly raises a fundamental question: is the failure of roughness estimation for Bitcoin a finite-sample artefact, a manifestation of market-specific features such as multifractality, or evidence that rough volatility models are structurally incompatible with this asset class? Resolving this question is central to understanding the volatility dynamics of cryptocurrency markets and to evaluating the broader applicability of rough volatility models beyond traditional financial assets.

## 1.4 Hypotheses

We formulate the following working hypotheses to guide our empirical investigation:

**H1. Bitcoin volatility does not admit a global scaling law compatible with the normalised  $p$ -variation framework:**

Bitcoin volatility may not admit a well-defined global scaling law consistent with the assumptions of the normalised  $p$ -variation framework. Structural features such as microstructure noise, fragmented liquidity, and large volatility jumps can disrupt scaling regularity, making the estimation of a roughness index theoretically ill-posed. Empirically, this would manifest as a  $\log W(L, K, p)$  curve that fails to cross zero for any  $p$ .

**H2. Estimation Artefacts and Finite-Sample Effects:**

Even if rough scaling holds in principle, practical estimation may fail due to finite-sample distortions, data irregularities, or extreme returns. In this scenario, the systematic negativity of  $\log W(L, K, p)$  would indicate a breakdown of the estimator under limited or noisy data, rather than structural violations of scaling. This hypothesis attributes the failure to the method’s operational limitations, not to the underlying process.

**H3. Non-Stationarity or Regime Shifts:**

Bitcoin volatility may exhibit non-stationary or structural breaks, violating key assumptions of the  $p$ -variation estimator. Regime changes, persistent trends, or time-varying scaling could compromise the interpretability of the  $W(L, K, p)$  statistic. We assess this hypothesis by applying the Augmented Dickey-Fuller (ADF) test for unit roots, computing rolling mean and variance statistics to evaluate local stability, and detecting structural breaks using binary segmentation with an  $L_2$ -based cost function, as detailed in Section 3.6.1.

**H4. Multifractality of Bitcoin Volatility:**

Bitcoin volatility may exhibit an inherently multifractal temporal structure, where different segments exhibit varying local scaling exponents. This heterogeneity precludes the existence of a single global roughness index and is incompatible with the normalised  $p$ -variation framework. We investigate this hypothesis using complementary diagnostics: Multifractal Detrended Fluctuation Analysis (MF-DFA), log-log scaling of moments, and Wavelet Leaders Multifractal Analysis.

## 1.5 Contributions

This study makes three contributions to the literature on volatility modelling and the structural properties of cryptocurrency markets.

First, it offers an extensive application of the normalised  $p$ -variation framework to Bitcoin realised volatility across multiple years and sampling frequencies, making the analysis more comprehensive than any prior roughness estimation in cryptocurrency markets. The analysis reveals a systematic and robust failure of roughness estimation across all empirical configurations.

Second, we demonstrate that the failure of roughness estimation cannot be attributed to finite-sample effects or non-stationarity. Extensive stationarity tests and window stability analyses exclude estimation artefacts and regime changes. Multifractal diagnostics, namely Multifractal Detrended Fluctuation Analysis, log-log moment scaling, and wavelet leaders analysis, based on established fractal analysis methods Kantelhardt et al. (2002); Wendt et al. (2007), confirm that Bitcoin volatility exhibits a multifractal temporal structure. This structure is incompatible with the homogeneous scaling assumptions required by rough volatility models.

Third, the results contribute to the evaluation of the rough volatility paradigm by showing that, while effective in equity and foreign exchange markets, rough stochastic volatility models face structural challenges when applied to Bitcoin realised volatility. This finding underscores the need for models that explicitly incorporate multifractal and scale-dependent dynamics to capture the unique characteristics of cryptocurrency markets. Examples of such alternatives include the Multifractal Random Walk Bacry et al. (2001) and Multifractal Stochastic Volatility Calvet and Fisher (2002) models.

## 2 Literature Review

### 2.1 Rough Volatility and the Hurst Paradigm

The rough volatility paradigm models financial market volatility as a stochastic process whose sample paths are rougher than those of Brownian motion. Motivated by empirical evidence that volatility exhibits low Hölder regularity at high frequencies, this approach posits that volatility dynamics are well described by fractional processes with Hurst exponents  $H < 0.5$  Gatheral et al. (2018). In such models, volatility paths display pronounced fine-scale irregularity (indicative of low short-term regularity) but not necessarily long-range dependence. This roughness aligns with the volatility clustering and persistent fluctuations observed in high-frequency equity market data.

Empirical support for the rough volatility hypothesis has emerged from multiple methodological approaches. These include the log-regression of realised volatility increments Gatheral et al. (2018), parametric estimation of fractional stochastic volatility models Fukasawa et al. (2022), and non-parametric diagnostics based on  $p$ -variation Cont and Das (2024). Across these methods, estimated Hurst exponents in equity and index markets typically fall in the range 0.1 to 0.3. These findings have motivated the adoption of rough stochastic volatility models, originally proposed by Gatheral and Rosenbaum and empirically validated by Bennedsen, Lunde, and Pakkanen Bennedsen et al. (2016), in both academic research and quantitative finance practice. Rough models have demonstrated empirical success in capturing the fine-scale behaviour of implied volatility surfaces and short-term volatility dynamics.

The applicability of the rough volatility paradigm across asset classes remains contested. Rogers (2019) and Cont and Das (2024) have emphasised that low roughness estimates derived from realised volatility may not reflect intrinsic properties of the spot volatility process, but instead result from structural features of the data or estimation artefacts. For example, Rogers (2019) showed that microstructure noise or irregular sampling can generate artificially low Hurst exponents, cautioning against interpreting realised path roughness as direct evidence of true volatility roughness. These confounding effects, including multifractal scaling, may induce apparent roughness even when the underlying volatility process is not genuinely rough. This underscores the need for model-free diagnostics when extending rough volatility models beyond traditional markets.

### 2.2 The Cont–Das Normalised $p$ -Variation Estimator

To address the limitations of traditional approaches, we adopt the framework introduced by Cont and Das (2024). This framework provides a model-free, pathwise-consistent estimator of roughness based on the scaling behaviour of the normalised  $p$ -variation statistic

$W(L, K, p)$ , computed over a sequence of block partitions of the observed time series. Intuitively,  $W(L, K, p)$  measures how the  $p$ -th variation of the process accumulates across blocks, normalised in such a way that for a self-similar process with a global scaling law, the statistic equals one exactly at the correct scaling exponent  $p^*$ . Thus, plotting  $\log W(L, K, p)$  as a function of  $1/p$ , one expects a zero-crossing at a unique value  $p = p^*$ , which defines the variation index and yields the corresponding roughness index  $H = 1/p^*$ . The existence of this zero-crossing serves as a rigorous criterion for determining whether the process admits a global monofractal scaling regime consistent with Hölder-type roughness. For reference, the formal definition of  $W(L, K, p)$  is provided in Section 3.1.

The normalised  $p$ -variation estimator is non-parametric, robust to non-Gaussian features, and directly applicable to realised volatility series. It serves not only as a roughness estimator but also as a structural diagnostic of the underlying process. Specifically, the presence or absence of a zero-crossing in  $\log W(L, K, p)$  determines whether the data admit a well-defined global scaling law consistent with the rough volatility paradigm. If no zero-crossing is observed, it implies that no single roughness exponent can characterise the process, indicating a fundamental incompatibility with monofractal scaling assumptions.

Recent applications of the method to equity markets have validated its efficacy Cont and Das (2024), producing roughness estimates consistent with the existing literature. In particular, Cont and Das apply the normalised  $p$ -variation estimator to 5-minute realised volatility of the S&P 500 using the Oxford-Man Institute dataset. They observe a well-defined zero-crossing in  $\log W(L, K, p)$ , with the resulting roughness index estimated in the range  $H \in [0.05, 0.25]$ , consistent with prior findings from log-regression methods.

## 2.3 Multifractality in Financial Time Series

Multifractality characterises time series in which different segments exhibit heterogeneous local scaling behaviour, thereby precluding the existence of a single global scaling exponent. In such processes, the scaling exponents vary continuously with the moment order, leading to non-linear moment scaling functions or curvature in the wavelet spectrum Bacry et al. (2001); Calvet and Fisher (2002). This stands in contrast to monofractal processes, which are governed by a single exponent that applies uniformly across all time scales and moments.

Empirical research has established that financial time series often exhibit multifractal properties. Foundational models such as the Multifractal Random Walk Bacry et al. (2001) and the Multifractal Stochastic Volatility model Calvet and Fisher (2002) account for stylised features such as volatility clustering, heavy tails, and long memory through underlying multifractal dynamics. Subsequent studies have confirmed these properties across equities, foreign exchange, and commodities. More recent work has extended this evidence to cryptocurrencies. High-frequency Bitcoin returns and trading volume exhibit multifractal scaling when analysed using Multifractal Detrended Fluctuation Analysis Mensi et al. (2019); Matteo (2007), and complex multiscale dependence has been observed in cross-correlation structures Watorek et al. (2022). Additional research shows that Bitcoin realised volatility also displays a multifractal structure, though weaker than that of returns Zhou et al. (2022). These findings support the view that multifractality is a robust and persistent feature of financial markets and offer a plausible explanation for the structural deviations from monofractal scaling observed in Bitcoin volatility.

Multifractality is fundamentally incompatible with the rough volatility paradigm,

which assumes homogeneous Hölder regularity across scales. A multifractal process does not admit a single Hurst exponent, its apparent roughness varies with the moment order or temporal scale considered. As a result, roughness estimators based on global scaling laws, such as the normalised  $p$ -variation estimator, are theoretically ill-posed in this context and may yield misleading conclusions. In such settings, the absence of a well-defined roughness index is not a limitation of the estimator but reflects a structural property of the underlying process Cont and Das (2024).

## 3 Data and Methodology

### 3.1 Mathematical Framework

#### $p$ -Variation and Hölder Regularity:

Let  $X = \{X_t\}_{t=1}^L$  be a real-valued function or time series. Its  $p$ -variation over the discrete index set  $\{1, \dots, L\}$  is defined as

$$V_p(X) = \sup_{\mathcal{P}} \sum_{i=1}^n |X_{t_i} - X_{t_{i-1}}|^p, \quad (1)$$

where the supremum is taken over all finite partitions  $\mathcal{P} = \{0 = t_0 < t_1 < \dots < t_n = L\}$ . If  $V_p(X) < \infty$ , we say that  $X$  has finite  $p$ -variation.

A related concept is the *Hölder exponent*  $H \in (0, 1)$ , which characterises the local regularity of  $X$  via the condition

$$|X_t - X_s| \leq C|t - s|^H \quad \text{for all } s, t \text{ in a neighborhood.}$$

Smaller values of  $H$  correspond to rougher paths. Brownian motion has  $H = 0.5$ , while rough volatility models typically assume  $H \in (0.1, 0.4)$ . The roughness index we estimate serves as a nonparametric proxy for local Hölder regularity.

#### Normalised $p$ -Variation and Roughness Index:

Let  $X = \{X_t\}_{t=1}^L$  denote a discrete time series with  $L$  observations. Given a partition of  $X$  into  $K$  consecutive, non-overlapping blocks of size  $n = L/K$ , define the block sums  $S_j = \sum_{i=(j-1)n+1}^{jn} X_i$  for  $j = 1, \dots, K$ .

The *normalised  $p$ -variation statistic* is then defined as

$$W(L, K, p) = \frac{1}{K} \sum_{j=1}^K |S_j|^p. \quad (2)$$

For a process exhibiting homogeneous scaling,  $\log W(L, K, p)$  is expected to be strictly decreasing in  $1/p$  and to cross zero at a unique value  $p = p^*$  such that  $W(L, K, p^*) = 1$ . The *roughness index* is then defined as

$$\hat{H} = \frac{1}{p^*}. \quad (3)$$

This index  $\hat{H}$  captures the fine-scale regularity of the path  $X$ . A value  $\hat{H} < 0.5$  indicates rougher-than-Brownian behaviour. This construction forms the basis of the normalised  $p$ -variation estimator of Cont and Das (2024), which detects roughness by identifying the moment  $p^*$  at which the aggregated variation normalises. The estimate

$\hat{H} = 1/p^*$  serves as a nonparametric, model-free proxy for the path’s Hölder-type regularity.

### Multifractality and Scaling Exponents:

A stochastic process  $X = \{X_t\}_{t=1}^L$  is said to exhibit multifractality if its scaling behaviour varies with the moment order  $q$ . This is characterised by a non-linear dependence of structure function exponents on  $q$ .

*Log-moment scaling* diagnostics evaluate the empirical relation

$$M_q(\tau) = \mathbb{E}[|X_{t+\tau} - X_t|^q] \sim \tau^{\zeta_q}, \quad (4)$$

where  $\zeta_q$  is the  $q$ -th order scaling exponent and  $\tau$  denotes the time scale. In practice,  $\zeta_q$  is estimated by regressing  $\log M_q(\tau)$  on  $\log \tau$  over a range of scales. Multifractality is indicated by the non-linearity of the  $\zeta_q$  curve in  $q$ , monofractal processes correspond to linear  $\zeta_q$ .

*Multifractal detrended fluctuation analysis (MF-DFA)* estimates the generalised Hurst exponent  $H(q)$  via the relation

$$F_q(s) \sim s^{H(q)}, \quad (5)$$

where  $F_q(s)$  is the  $q$ -th order fluctuation function over window size  $s$ . As with  $\zeta_q$ , curvature in  $H(q)$  implies multifractality, while constancy indicates monofractal behaviour.

*Wavelet leaders multifractal analysis* estimates scaling via the moments of wavelet leader coefficients  $d_{j,k}$  at scale  $2^j$ :

$$\mathbb{E}[|d_{j,k}|^q] \sim 2^{j\zeta_q}. \quad (6)$$

Linear regression of  $\log_2 \mathbb{E}[|d_{j,k}|^q]$  on  $j$  yields  $\zeta_q$ , and the width  $\zeta_{\max} - \zeta_{\min}$  serves as a summary statistic for the strength of multifractality. As a scalar diagnostic, we compute the *spectrum width* defined as  $\zeta_{q_{\max}} - \zeta_{q_{\min}}$ , typically over  $q \in [-4, +4]$ . Larger widths indicate stronger multifractal heterogeneity.

Across all methods, multifractality is diagnosed through the non-linearity and spectrum width of  $q \mapsto H(q)$  or  $q \mapsto \zeta_q$ , reflecting the heterogeneity of local scaling exponents. These diagnostics are applied over appropriate intermediate scales by selecting intermediate time scales that avoid both microstructure noise (short scales) and non-stationary drift (long scales) (see Kantelhardt et al. (2002) for MF-DFA and Wendt et al. (2007) for wavelet leader analysis). The definitions presented in this section underpin the empirical diagnostics and estimation procedures reported in Sections 3.6.2 and 4.3.

## 3.2 Data Description and Preprocessing

This study employs a high-frequency dataset of BTC/USD prices recorded at one-minute intervals, derived from the publicly available “Bitcoin Historical Data” dataset on Kaggle. The dataset aggregates minute-level transaction data from the Bitstamp exchange via its public API. The full dataset spans from January 2012 to May 2025 and includes open, high, low, and close prices, along with traded volume in BTC, timestamped in UTC. It is updated daily through an automated pipeline hosted on GitHub Actions, which retrieves and integrates historical data directly from Bitstamp.

Although the dataset includes automated deduplication and merge routines, its documentation acknowledges potential limitations in data completeness and consistency, including gaps due to exchange outages or API availability. No formal data validation

is provided. To mitigate these issues, we restrict our analysis to the 2017-2024 period, during which data quality is sufficiently stable for high-frequency volatility estimation.

To ensure consistency and minimise missing data effects, for each calendar year  $Y$ , we systematically selected the most complete 90-day window of consecutive minute-level BTC/USD observations. We opted to analyse one representative 90-day high-quality segment per year to control for seasonality and to ensure stationarity over each segment. Using longer or multiple windows risked including structural changes or requiring imputation for extensive gaps. Let  $T = 129,600$  minutes denote the target window length. The search space was defined as the set of all candidate windows of length  $T$ , starting at time  $t_s$  and ending at  $t_e = t_s + T - 1$ , with  $t_s$  incremented in daily steps (1,440 minutes). For each candidate window, we constructed the corresponding sequence of timestamps  $\{t_i\}_{i=1}^T$  and computed the number of missing Close price observations  $m(t_s)$ . The optimal window  $[t_s^*, t_e^*]$  was selected as:

$$(t_s^*, t_e^*) = \arg \min_{t_s} m(t_s)$$

In the event of ties, where multiple windows contained the same minimum number of missing observations, the most recent window was selected. Years in which no complete 90-day window was available were excluded from further analysis. The selected windows serve as the basis for the annual volatility estimation pipeline.

For each target frequency  $f \in 5, 10, 15$  minutes, resampling was conducted as follows. The original 1-minute series was first filtered to exclude zero-volume minutes. Aggregated bars were then constructed using standard OHLCV conventions: the *Open* price corresponds to the first valid price within the interval; the *High* and *Low* are, respectively, the maximum and minimum prices observed; the *Close* is the last valid price; and the *Volume* is computed as the sum of traded volume over the interval.

To prevent bias from incomplete interval aggregation, only intervals containing exactly  $N_f$  valid 1-minute observations were retained, where  $N_f = f$ . Intervals with missing observations were discarded.

To ensure high data quality for volatility estimation, a completeness filter was applied after resampling. For each (year, frequency) pair, we computed the completeness ratio as the percentage of expected time intervals for which a valid OHLCV bar was present. Only windows with completeness above 90% were retained:

$$\text{Completeness}(Y, f) = \frac{N_{\text{valid}}(Y, f)}{N_{\text{expected}}(f)} \times 100\%$$

where  $N_{\text{expected}}(f)$  is the theoretical number of bars at frequency  $f$  for a 90-day window, and  $N_{\text{valid}}(Y, f)$  is the number of valid, fully aggregated bars.

Finally, for each retained window, any remaining observations with missing values were removed via listwise deletion. The resulting datasets consist exclusively of complete, uniformly sampled OHLCV bars. These cleaned series served as direct inputs for volatility estimation and multifractal analysis.

The completeness statistics computed as described above are reported in Table 1.

Table 1: Completeness of selected 90-day Bitcoin data windows (2017-2024).

Year	Frequency	Valid Bars	Expected Bars	Completeness (%)
2017	1-min	128,014	129,600	98.78
	5-min	24,665	25,920	95.16
	10-min	11,883	12,960	91.69
	15-min	7,697	8,640	89.09
2018	1-min	129,180	129,600	99.68
	5-min	25,543	25,920	98.55
	10-min	12,610	12,960	97.30
	15-min	8,319	8,640	96.28
2019	1-min	128,999	129,600	99.54
	5-min	25,422	25,920	98.08
	10-min	12,501	12,960	96.46
	15-min	8,205	8,640	94.97
2020	1-min	128,998	129,600	99.54
	5-min	25,379	25,920	97.91
	10-min	12,461	12,960	96.15
	15-min	8,179	8,640	94.66
2021	1-min	129,464	129,600	99.90
	5-min	25,795	25,920	99.52
	10-min	12,837	12,960	99.05
	15-min	8,520	8,640	98.61
2022	1-min	127,584	129,600	98.44
	5-min	24,267	25,920	93.62
	10-min	11,486	12,960	88.63
	15-min	7,280	8,640	84.26
2023	1-min	126,682	129,600	97.75
	5-min	23,462	25,920	90.52
	10-min	10,784	12,960	83.21
	15-min	6,677	8,640	77.28
2024	1-min	128,503	129,600	99.15
	5-min	25,052	25,920	96.65
	10-min	12,184	12,960	94.01
	15-min	7,927	8,640	91.75

A 90% completeness threshold was imposed at each frequency to balance data quality with temporal coverage. For 1-minute and 5-minute data, all years from 2017 to 2024 met this criterion. For 10-minute data, 2022 and 2023 were excluded, while for 15-minute data, 2017, 2022, and 2023 were excluded. The remaining data were sufficient to observe clear patterns, and no contradictory behaviour was seen in partially excluded years at other frequencies. The complete list of retained and excluded years is given in Appendix Table A.1.

No interpolation or imputation was performed at any stage. Missing data were handled exclusively by window selection and exclusion, preserving the integrity of volatility

estimates and avoiding artefactual smoothing.

Temporal structure and integrity of each retained window were further assessed. Large temporal gaps, defined as sequences of missing data exceeding one hour, were systematically identified at each frequency. Such gaps were rare for 1-minute and 5-minute data, but more common at coarser resolutions, especially in early years and in 2024. Full gap statistics are provided in Appendix Table A.2.

Integrity checks were conducted to confirm the suitability of the data for volatility modelling. These included confirming the absence of residual missing values after complete-case filtering, ensuring that all closing prices were strictly positive and non-missing, and verifying that timestamp sequences were strictly increasing to preserve temporal alignment.

For each frequency, closing prices are first transformed into log-returns, defined as the first difference of the natural logarithm of consecutive closing prices:

$$r_t = \log S_t - \log S_{t-1}$$

where  $S_t$  denotes the closing price at time  $t$ . The log-return series is computed separately for each calendar year and each frequency, yielding one series per (year, frequency) pair.

Prior to volatility estimation, each log-return series was screened for data quality issues and extreme values. An absolute threshold test is applied: any return exceeding  $|r_t| > 0.2$  (approximately 22%) is flagged. Statistical outliers are identified using a  $z$ -score criterion with a threshold of six standard deviations from the mean.

$Z$ -score histograms and Q-Q plots, shown in Appendix Figures B.4-B.6 and B.1-B.3, reveal that Bitcoin log-returns exhibit strong leptokurtosis and significant departures from Gaussianity across all year and frequency configurations. These deviations intensify at higher sampling frequencies, where extreme quantiles diverge markedly from the normal benchmark. The presence of heavy tails suggests that moment-based scaling diagnostics may be sensitive to outliers. To preserve the true structure of return variability, we retain all observations and later apply a shuffle-resampling approach to disentangle heavy-tail effects from temporal dependence in our multifractality tests.

No filtering was applied beyond the initial screening, all flagged returns were retained, and no values were removed or modified.

### 3.3 Realised Volatility Construction

For each year and frequency configuration, we define a proxy for high-frequency volatility by taking the modulus of log-returns at the original sampling resolution. Let  $\{r_t\}_{t=1}^L$  denote the log-return series over a 90-day window, where  $L$  is the number of observations. We define the pointwise volatility proxy as

$$RV_t = |r_t|, \quad t = 1, \dots, L.$$

This absolute return series preserves the temporal resolution of the data and captures the local magnitude of return fluctuations. For notational convenience, we refer to  $\{RV_t\}$  as the realised volatility series, although it is more accurately a proxy for instantaneous volatility rather than an integrated measure.

Formally, for sampling frequency  $f$  and year  $Y$ , let  $X(f, Y) = \{r_t(f, Y)\}_{t=1}^{L_{f,Y}}$  denote the log-return series. We construct

$$RV(f, Y) = \{|r_t(f, Y)|\}_{t=1}^{L_{f,Y}},$$

where  $L_{f,Y}$  is the number of valid observations in the selected window. This operation is applied uniformly across all configurations to produce a consistent panel of absolute return series for nonparametric roughness estimation.

We use absolute returns rather than squared returns since the normalised  $p$ -variation estimator can be directly applied to any  $L^p$ -type measure. The absolute value provides a fat-tailed yet finite input and is more robust to extreme values. Accordingly, we estimate the Hölder roughness of the volatility path itself (as captured by absolute returns), rather than of the price or log-price process. Working directly with the raw volatility magnitude series avoids imposing lognormality or continuous-time modelling assumptions. This follows the approach of Gatheral et al. (2018) and Cont and Das (2024), who focus on volatility time series for roughness estimation.

A potential concern, highlighted in Fukasawa et al. (2022), is that realized volatility constructed from single low-frequency returns

$$RV_t^\Delta = |r_{t,\Delta}|$$

may be contaminated by white-noise components, leading to artificially rough behaviour. To address this, we also consider a noise-robust construction: for each frequency  $\Delta$ , one realized volatility observation is computed as

$$\widetilde{RV}_t^\Delta = \left( \sum_{i=1}^{\Delta} r_{t,i}^2 \right)^{1/2},$$

where  $\{r_{t,i}\}$  are one-minute log-returns within the  $\Delta$ -minute interval. This definition ensures that each volatility estimate incorporates multiple high-frequency increments, thereby mitigating the influence of white-noise domination. As reported in Appendix A.12, the use of  $\widetilde{RV}_t^\Delta$  does not alter our main findings: the statistic  $W(p)$  remains strictly negative across all years and frequencies, indicating that the absence of a zero-crossing cannot be explained by noise contamination alone.

### 3.4 Diagnostic Exploration: Roughness vs $K$

Prior to finalising the roughness estimation procedure, we conduct a diagnostic analysis to examine how the estimated roughness  $H_{L,K}$  depends on the number of blocks  $K$  (which controls the partition size). This step ensures we choose an appropriate  $K$  for each case, as the estimate can be sensitive to this choice. The diagnostic analysis evaluates the behaviour of the roughness estimator  $\widehat{H}^{L,K}$  as a function of the number of blocks  $K$ .

For each calendar year and sampling frequency,  $\widehat{H}^{L,K}$  is computed over a wide range of  $K$  values, starting from  $K = 50$ , with frequency-specific grid steps to ensure robust coverage of the admissible  $K$  range given the sample size. The estimator follows the normalised  $p$ -variation methodology, computed using block-summed returns and linear regression of  $\log W(L, K, p)$  on  $1/p$ .

Diagnostic plots of  $\widehat{H}^{L,K}$  versus  $K$  were generated for each (year, frequency) pair. See Section 4.1 for representative results. Across all configurations, these diagnostic plots consistently reveal substantial instability of  $\widehat{H}^{L,K}$  as a function of  $K$ , underscoring the need for principled block size selection.

In principle, a small  $K$  leads to highly variable estimates due to insufficient averaging, while a very large  $K$  may induce bias by under-representing the high-frequency components of the process. As such, no single value of  $K$  ensures consistency in finite samples,

and the behaviour of  $\widehat{H}^{L,K}$  as a function of  $K$  must be carefully examined. Accordingly, the  $\widehat{H}^{L,K}$  plot as a function of  $K$  is not expected to be flat or perfectly stable, as changes in  $K$  inherently induce fluctuations in the estimate due to the bias-variance trade-off.

To mitigate these issues, Cont and Das (2024) recommend selecting  $K$  such that  $K \approx \sqrt{L}$ , where  $L$  is the number of available observations. This choice ensures a trade-off between bias and variance, grounded in the theoretical convergence properties of the normalised  $p$ -variation statistic:

$$\lim_{K \rightarrow \infty} \lim_{L \rightarrow \infty} W(L, K, p) \rightarrow w(x, p, \pi) \quad (7)$$

and maintains a sufficient block size  $n = L/K$  to stabilise the estimation.

Following the recommendation of Cont and Das (2024), we set  $K_{\text{opt}} = \lfloor \sqrt{N} \rfloor$ , where  $N$  is the number of realised volatility observations for the given year and frequency. The corresponding block size is set to  $n_{\text{opt}} = K_{\text{opt}}$ , ensuring an equal partition. This results in  $L = K_{\text{opt}} \times n_{\text{opt}}$  data points used in the estimation. When necessary, a few observations are discarded to make  $L$  exactly divisible by  $K_{\text{opt}}$ . Table 2 reports the resulting partition parameters for each year and frequency.

Table 2: Summary of sample sizes and partitioning parameters  $(K, n, L)$  per year and frequency. For each (year, frequency) pair,  $K_{\text{opt}} = n_{\text{opt}} = \lfloor \sqrt{N} \rfloor$  and  $L = K \times n$  is the number of data points used in estimation.

Frequency	Year	$N_{\text{points}}$	$K_{\text{opt}}$	$n_{\text{opt}}$	$L$
1-min	2017	128013	357	357	127449
1-min	2018	129179	359	359	128881
1-min	2019	128998	359	359	128881
1-min	2020	128997	359	359	128881
1-min	2021	129463	359	359	128881
1-min	2022	127583	357	357	127449
1-min	2023	126681	355	355	126025
1-min	2024	128502	358	358	128164
5-min	2017	24664	157	157	24649
5-min	2018	25542	159	159	25281
5-min	2019	25421	159	159	25281
5-min	2020	25378	159	159	25281
5-min	2021	25794	160	160	25600
5-min	2022	24266	155	155	24025
5-min	2023	23461	153	153	23409
5-min	2024	25051	158	158	24964
10-min	2017	11882	109	109	11881
10-min	2018	12609	112	112	12544
10-min	2019	12500	111	111	12321
10-min	2020	12460	111	111	12321
10-min	2021	12836	113	113	12769
10-min	2024	12183	110	110	12100
15-min	2018	8318	91	91	8281
15-min	2019	8204	90	90	8100
15-min	2020	8178	90	90	8100
15-min	2021	8519	92	92	8464
15-min	2024	7926	89	89	7921

At the 1-minute frequency,  $K_{\text{opt}}$  typically ranges from 355 to 359, whereas at the 15-minute frequency it ranges from 89 to 92. The corresponding number of observations  $L$  used in estimation is slightly below the total  $N$  due to truncation, which ensures exact partitioning. For example, in 2017 at the 1-minute frequency, only 0.4% of the data is discarded to ensure that  $L = K \times n$  holds exactly. These adjustments are minimal and do not materially affect the estimation procedure.

This approach ensures that the roughness estimates rely on stable and theoretically grounded choices of  $K$ , enabling consistent comparisons across years and frequencies. Given the high-frequency sampling and large sample sizes, the normalised  $p$ -variation estimator operates within the asymptotic regime necessary for its consistency, as established in Cont and Das (2024). To assess estimator behaviour, we additionally inspected the curvature and zero-crossing properties of the  $\log W(L, K, p)$  curves across a grid of  $p$  values. In Section 3.5, we proceed to compute and analyse the final roughness estimates using these  $K_{\text{opt}}$  values.

### 3.5 Final Estimation Setup

For each (year, frequency) pair, we use the optimal block parameters  $(K, n)$  determined in Section 3.4. The block sums  $S_j$  are computed, and the normalised  $p$ -variation statistic is evaluated as:

$$W(L, K, p) = \frac{1}{K} \sum_{j=1}^K |S_j|^p. \quad (8)$$

To explore the robustness of our estimation and the stability of roughness behaviour, we compute  $W(L, K, p)$  over two grids of  $p$ . The first is a standard grid, defined as  $p \in [0.1, 4.0]$ , as originally proposed by Cont and Das (2024). The second is an extended exploratory grid (hereafter referred to as the “wide” grid), defined as  $p \in [0.01, 4.0]$ , allowing finer resolution of estimator behaviour at small  $p$  values.

For each configuration, we plot  $\log W(L, K, p)$  against  $1/p$ , following standard diagnostic practice. The expected behaviour is a zero-crossing of  $\log W(L, K, p)$  at  $p = \hat{p}$ , which corresponds to the estimated variation index and yields the roughness estimator  $\hat{H} = 1/\hat{p}$ . This diagnostic behaviour is well-defined under the assumption that the process under study admits homogeneous scaling in the sense of Hölder-type regularity. The presence of a clear zero-crossing is a necessary condition for Bitcoin’s volatility to follow a rough volatility scaling law (Hypothesis H1).

Following Cont and Das (2024), we apply the estimator directly to the series of realised volatility magnitudes, defined as  $RV_t = |r_t|$ , where  $r_t$  is the log-return at time  $t$ . This approach avoids any transformation to log-volatility or its increments, and the resulting roughness index  $\hat{H}$  captures the fine-scale regularity of the volatility path itself. Summary statistics of  $\log W(L, K, p)$  behaviour are reported in Table 3 in Section 4.1.

### 3.6 Diagnostic Tests

#### 3.6.1 Non-Stationarity Diagnostics

To assess whether the failure of the  $p$ -variation estimator may stem from non-stationarity or structural breaks, we apply three complementary diagnostics to each realised volatility series: the Augmented Dickey-Fuller (ADF) test for mean stationarity, rolling window analysis to evaluate local stability of mean and variance, and structural break detection to identify discrete regime shifts. Together, these methods provide a comprehensive assessment of both gradual and abrupt departures from stationarity.

Each diagnostic is applied independently to all combinations of year and sampling frequency. This convention is adopted throughout the remainder of this subsection and will not be restated for each method.

Unit root tests were conducted using the Augmented Dickey-Fuller (ADF) procedure. For each series, we estimate

$$\Delta RV_t = \alpha RV_{t-1} + \sum_{i=1}^p \beta_i \Delta RV_{t-i} + \varepsilon_t$$

with lag order  $p$  selected via the AIC criterion. The resulting test statistics and corresponding critical values are reported in Appendix Table A.3.

Rolling mean and variance stability were assessed by computing the standard deviation of rolling mean and variance estimates. We used a rolling window of length equal to

5% of the sample size (with a minimum of 10 observations). Specifically, we computed

$$\text{std}(\text{mean}_{t-w:t}(RV)), \quad \text{std}(\text{var}_{t-w:t}(RV))$$

where  $w$  denotes the rolling window length. The computed statistics are reported in Appendix Table A.4.

Structural breaks were detected using binary segmentation with an  $L_2$ -based cost function. We applied the algorithm with a maximum of five breakpoints per series, solving:

$$\min_{\tau_1, \dots, \tau_m} \sum_{k=0}^m \sum_{t=\tau_k+1}^{\tau_{k+1}} (RV_t - \mu_k)^2$$

where  $\{\tau_k\}$  are the breakpoints and  $\mu_k$  the segment means. The detected breakpoint indices are reported in Appendix Table A.5.

Overall, the applied diagnostics and their corresponding results are documented in Appendix Tables A.3, A.4, and A.5. These results will be interpreted in Section 4.2 to assess Hypothesis H3.

### 3.6.2 Multifractality Diagnostics

To assess whether Bitcoin’s realised volatility exhibits a multifractal temporal structure, we apply three complementary diagnostics: Multifractal Detrended Fluctuation Analysis (MF-DFA), log-log moment scaling, and wavelet leaders analysis. Each method is implemented systematically across all (year, frequency) combinations and applied uniformly to both log-return and realised volatility series. This convention is maintained throughout and not repeated in the descriptions that follow.

To isolate temporal dependence from distributional effects, we employ a shuffle-based robustness procedure: for each series, the time indices are randomly permuted, thereby removing temporal correlations while preserving the marginal distribution. Comparisons between original and shuffled series allow us to attribute multifractal signatures specifically to dynamic rather than distributional structure.

Multifractal Detrended Fluctuation Analysis (MF-DFA) estimates the generalised Hurst exponent  $H(q)$  over the moment range  $q \in [-4, 4]$ , following standard MF-DFA methodology. Specifically, for each  $q$ , the slope of the log-log regression

$$\log F_q(s) \sim H(q) \log s$$

is computed, where  $F_q(s)$  denotes the  $q$ th-order fluctuation function at scale  $s$ . Summary statistics for the resulting  $H(q)$  spectra (including minimum, maximum, mean, and spectral width) are reported in Appendix Table A.6 (log-returns) and Table A.9 (realised volatility).

Log-log moment scaling analysis is used to estimate empirical scaling exponents  $\zeta_q$  by computing, for each moment order  $q \in [-4, 4]$ , the slope of the scaling relation

$$\log M_q(\tau) \sim \zeta_q \log \tau$$

is computed, where  $M_q(\tau)$  denotes the  $q$ th-order moment of increments at lag  $\tau$ . This procedure is implemented over a dense grid of lags  $\tau$ . Complete results are presented in Appendix Table A.7 (log-returns) and Table A.10 (realised volatility).

Wavelet leaders multifractal analysis estimates the scaling relation for each moment order  $q \in [-4, 4]$ , the scaling relation

$$\log_2 M_q(2^j) \sim \zeta_q j$$

is estimated, where  $M_q(2^j)$  denotes the  $q$ th-order moment of wavelet leaders at dyadic scale  $2^j$ . Scaling exponents  $\zeta_q$  are obtained via linear regression, and corresponding  $R^2$  values are recorded to evaluate the quality of fit. Wavelet leaders, constructed from the local suprema of wavelet coefficients across scales, offer robustness to non-stationarities and facilitate the isolation of multiscale fluctuations from deterministic trends. Full results are presented in Appendix Table A.8 (log-returns) and Table A.11 (realised volatility).

A non-linear relationship between  $H(q)$  or  $\zeta_q$  and the moment order  $q$  is a hallmark of multifractality, indicating scale-dependent dynamics. The reduction in multifractal spectrum widths observed in the shuffled data serves as a robustness check, indicating that the multifractality originates from temporal correlations rather than from the heavy-tailed distribution of volatility increments.

## 4 Empirical Results

### 4.1 Main Result: Roughness Estimation behaviour

We now analyse the behaviour of the normalised  $p$ -variation statistic  $\log W(L, K, p)$  across all (year, frequency) pairs of the dataset.

As detailed in Section 3.4, examining the behaviour of  $\widehat{H}^{L,K}$  across varying  $K$  offers diagnostic insight into scaling stability and guides the selection of a robust block size.

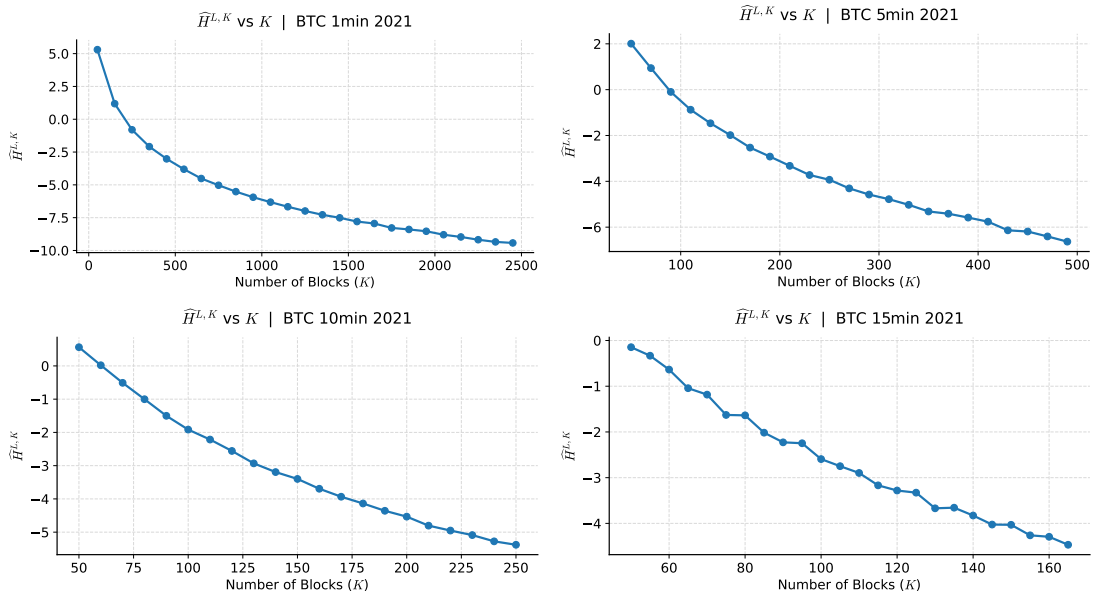


Figure 1: Estimated roughness index  $\widehat{H}^{L,K}$  versus number of blocks  $K$  for BTC realised volatility in 2021 at 1-minute (top-left), 5-minute (top-right), 10-minute (bottom-left), and 15-minute (bottom-right) frequencies.

As shown in Figure 1, for the 1-minute data,  $\widehat{H}^{L,K}$  is clearly positive for small  $K$  (up to approximately  $K \approx 200$ ) and then declines sharply, becoming negative for larger

$K$ . The 5-minute series exhibits a qualitatively similar pattern, with positive values at low  $K$  and a progressive decrease. In contrast, for the 10-minute and 15-minute series,  $\widehat{H}^{L,K}$  remains strictly negative throughout the entire  $K$ -range. In practice, we observed that  $\widehat{H}_{L,K}$  tends to be inflated when  $K$  is small, reflecting high estimator variance due to coarse partitioning. As  $K$  increases, the estimator often fails to return a value, since  $\log W(L, K, p)$  remains strictly negative and no zero-crossing is detected. This pattern reflects a fundamental bias-variance trade-off: small  $K$  amplifies stochastic variability, while large  $K$  discards fine-scale information necessary for identifying path roughness. It emphasises the need for principled selection of  $K$ , as arbitrary choices can produce misleading indications of roughness at small scales. To address this, the final roughness estimates are based on the theoretically justified criterion  $K_{\text{opt}} \approx \sqrt{N}$ .

Using the optimal partition size  $K_{\text{opt}} \approx \sqrt{N}$ , as derived in Section 3.4, we compute the normalised  $p$ -variation statistic  $\log W(L, K, p)$  for all (year, frequency) pairs across a wide range of  $p$ , following the final estimation procedure of Section 3.5. The summary of minimum and maximum values of  $\log W(L, K, p)$  is presented in Table 3.

Table 3: Minimum and maximum values of  $\log W(L, K, p)$  for each (frequency, year) pair, for both standard and wide grids.

Frequency	Year	Standard Grid		wide Grid	
		Min	Max	Min	Max
1min	2017	-1.797	-0.090	-1.797	-0.009
1min	2018	-3.454	-0.110	-3.454	-0.011
1min	2019	-3.149	-0.114	-3.149	-0.011
1min	2020	-1.857	-0.124	-1.857	-0.012
1min	2021	-2.377	-0.098	-2.377	-0.010
1min	2022	-5.021	-0.154	-5.021	-0.015
1min	2023	-6.177	-0.199	-6.177	-0.020
1min	2024	-5.249	-0.175	-5.249	-0.018
5min	2017	-1.636	-0.091	-1.636	-0.009
5min	2018	-3.778	-0.119	-3.778	-0.012
5min	2019	-3.206	-0.120	-3.206	-0.012
5min	2020	-1.911	-0.142	-1.911	-0.014
5min	2021	-2.438	-0.100	-2.438	-0.010
5min	2022	-5.230	-0.154	-5.230	-0.015
5min	2023	-6.375	-0.190	-6.375	-0.019
5min	2024	-5.502	-0.172	-5.502	-0.017
10min	2017	-1.612	-0.090	-1.613	-0.009
10min	2018	-3.866	-0.121	-3.866	-0.012
10min	2019	-3.382	-0.122	-3.382	-0.012
10min	2020	-2.012	-0.147	-2.012	-0.015
10min	2021	-2.577	-0.100	-2.577	-0.010
10min	2024	-5.560	-0.170	-5.560	-0.017
15min	2018	-3.867	-0.123	-3.867	-0.012
15min	2019	-3.358	-0.123	-3.358	-0.012
15min	2020	-2.091	-0.149	-2.091	-0.015
15min	2021	-2.545	-0.100	-2.545	-0.010
15min	2024	-5.544	-0.170	-5.544	-0.017

As shown in Table 3,  $\log W(L, K, p)$  remains strictly negative across all years, frequencies, and both the standard and extended  $p$ -grids. No zero-crossing is observed in any configuration, with maximum values not exceeding  $-0.009$ , even under the wide grid. This behaviour deviates from the expected pattern under homogeneous roughness, where a unique zero-crossing at  $p = \hat{p}$  would yield a well-defined roughness exponent  $H = 1/\hat{p}$ . The consistent absence of such a crossing indicates a systematic failure of the normalised  $p$ -variation estimator in the Bitcoin setting. The robustness of this result across years and frequencies suggests it reflects a structural property rather than a data artefact.

## 4.2 Stationarity and Window Stability

We begin by assessing whether non-stationarity could account for the anomalous behaviour of  $\log W(L, K, p)$ . Unit root tests were performed using the Augmented Dickey-Fuller (ADF) procedure as described in Section 3.6.1. The corresponding test statistics and  $p$ -values are reported in Appendix Table A.3. In all cases, the null hypothesis of a unit root is strongly rejected at the 5% significance level.

We next assess the local stability of the series by examining the rolling mean and variance statistics, following the procedure outlined in Section 3.6.1. Standard deviations of rolling means and variances were computed for each series, with results summarised in Appendix Table A.4. Across all frequencies and years, the rolling statistics exhibit low variability, indicating stable local behaviour. As expected, dispersion is marginally higher at coarser frequencies (10-minute and 15-minute), reflecting the aggregation of volatility rather than true non-stationarity. Crucially, no systematic trends or regime shifts are detected in the rolling statistics across all years and frequencies.

Finally, we detect structural breaks using binary segmentation with an  $L_2$ -based cost function, as described in Section 3.6.1. The identified breakpoints are reported in Appendix Table A.5. Breakpoints are detected in all series but predominantly align with periods of local volatility clustering. These breakpoints do not correspond to major regime shifts or persistent changes in volatility dynamics. Their occurrence is consistent with stationary behaviour exhibiting local clustering and does not indicate that structural instability accounts for the observed failure of the  $p$ -variation estimator.

Diagnostic results do not support non-stationarity or structural breaks as plausible explanations for the failure of the normalised  $p$ -variation estimator. Bitcoin realised volatility appears stationary with stable local dynamics. If non-stationarity were the cause, one would expect to observe systematic trends, level shifts, or persistent regime changes, none of which are observed in the diagnostic results.

## 4.3 Evidence of Multifractality

The results of the Multifractal Detrended Fluctuation Analysis (MF-DFA), described in Section 3.6.2, are reported in Appendix Tables A.6 and A.9. Across all original series, the estimated  $H(q)$  spectra exhibit pronounced non-linearity with respect to  $q$ , indicating scale-dependent behaviour characteristic of multifractality. For realised volatility,  $H(q)$  remain consistently below 1 across all years and sampling frequencies, typically centred around 0.9 for moderate  $q$ , with spectral widths between 0.06 and 0.42. Log-returns display lower mean exponents but retain comparable curvature in the scaling function. When applied to shuffled series, removing temporal structure while preserving the marginal distribution, the  $H(q)$  spectra compress substantially, with spectral widths falling below 0.15

in most cases. This contrast supports the interpretation that the observed multifractality arises from temporal dependence rather than distributional effects.

We next apply the log-log moment scaling analysis, an alternative multifractality diagnostic based on the scaling behaviour of  $\zeta_q$ , as described in Section 3.6.2. Estimated  $\zeta_q$  spectra for realised volatility and log-returns are presented in Appendix Tables A.7 and A.10. For realised volatility, the  $\zeta_q$  spectra exhibit pronounced curvature in  $q$ , with widths ranging from 0.04 to over 2.0 and mean  $R^2$  values generally exceeding 0.85, indicating stable scaling across temporal resolutions. Log-return series show more heterogeneity (especially at lower sampling frequencies) but maintain clear non-linearity in the  $\zeta_q$  profile for moderate to large  $q$ . In the shuffled series, the  $\zeta_q$  spectra flatten substantially, with widths typically below 0.2 and minimal curvature. These patterns are consistent with a temporal origin of the observed multifractality in both series.

The wavelet leaders multifractal analysis offers a robust characterisation of scaling behaviour, particularly in the presence of trends or non-stationarities. Estimated  $\zeta_q$  exponents for both realised volatility and log-return series are presented in Appendix Tables A.8 and A.11. For realised volatility, the  $\zeta_q$  spectra exhibit consistent curvature with spectral widths between 0.04 and 0.51 and mean  $R^2$  values typically exceeding 0.85. Log-return series show similar but generally weaker curvature, with greater sensitivity to sampling resolution. In the shuffled series, spectral widths decline substantially (often by more than 50%) and curvature is notably reduced.

The MF-DFA, log-log moment scaling, and wavelet leaders analyses consistently indicate that Bitcoin realised volatility exhibits a multifractal temporal structure. This conclusion is supported by the marked reduction in spectral curvature and width observed in shuffled controls, which preserve the marginal distribution but remove temporal dependence. These results suggest that the observed multifractality arises from temporal correlations rather than from heavy-tailed marginal distributions. This violates the homogeneity assumptions required by the normalised  $p$ -variation framework and provides a structural explanation for the failure to identify a well-defined scaling exponent. The apparent roughness at small  $q$  reflects localised scaling properties embedded in a broader multifractal structure, rather than a stable global Hurst exponent.

## 4.4 Hypothesis Evaluation

### **H1. Bitcoin volatility does not admit a global scaling law compatible with the normalised $p$ -variation framework:**

Our primary empirical result, the strict negativity of  $\log W(L, K, p)$  across all years, frequencies, and  $p$ -grids, demonstrates the absence of any stable scaling law compatible with the normalised  $p$ -variation estimator in Bitcoin realised volatility. This supports the interpretation that the apparent roughness reported in prior literature does not reflect an intrinsic property of the volatility process, but rather the failure of the  $p$ -variation framework to capture consistent scaling behaviour in this context. These findings confirm Hypothesis H1, as the strict negativity of  $\log W(L, K, p)$  across all configurations indicates the absence of a well-defined scaling law.

### **H2. Estimation Artefacts and Finite-Sample Effects:**

While finite-sample effects and estimation artefacts may contribute to the instability of the roughness estimator, they cannot fully account for the systematic and robust failure

observed here. The optimal partitioning strategy  $K \approx \sqrt{N}$ , validated in prior studies Cont and Das (2024), was applied consistently, and window stability diagnostics confirm that the input series meet the methodological requirements of the estimator. Market microstructure noise, irregular liquidity, and large volatility jumps, which are common in Bitcoin markets, likely exacerbate finite-sample distortions and further undermine the reliability of roughness estimation. However, finite-sample effects alone are insufficient to account for the observed empirical anomaly. We therefore reject  $H_2$  as a primary explanation, since finite-sample effects and estimation artefacts do not account for the systematic failure of  $\log W(L, K, p)$ .

### **H3. Non-Stationarity or Regime Shifts:**

Our suite of stationarity diagnostics, including the Augmented Dickey-Fuller test for unit roots, rolling mean and variance statistics for local stability, and structural break detection via binary segmentation with an  $L_2$ -based cost function, yields no evidence that non-stationarity or persistent structural instability accounts for the failure of the  $p$ -variation estimator. The realised volatility series are stationary over the studied periods, and the detected breakpoints correspond to local volatility clustering rather than structural regime changes. We therefore reject  $H_3$  as a primary explanation for the observed behaviour of  $\log W(L, K, p)$ , given the absence of non-stationarity or structural instability.

### **H4. Multifractality of Bitcoin Volatility:**

The multifractality hypothesis is decisively supported by our results. All three diagnostic approaches, MF-DFA, log-log moment scaling, and wavelet leaders analysis, exhibit consistent non-linear scaling in the original series and show substantial collapse of multifractal indicators under shuffle-based controls. This confirms that the observed multifractality in Bitcoin volatility, particularly in realised volatility, arises from genuine temporal correlations rather than from heavy-tailed marginal distributions. The presence of this multifractal temporal structure implies non-linear, scale-dependent behaviour that directly violates the homogeneity assumption of the normalised  $p$ -variation framework. We therefore accept  $H_4$  as the most plausible explanation for the observed behaviour of  $\log W(L, K, p)$ , as the multifractal structure of Bitcoin volatility is supported by all diagnostic results and offers a coherent account of the estimator’s failure.

## **5 Discussion**

### **5.1 Structural Interpretation**

Our analysis demonstrates that Bitcoin realised volatility exhibits pronounced scale dependence and temporal heterogeneity, in contrast to the patterns typically observed in traditional financial assets. Evidence from multiple diagnostics, reinforced by shuffled controls, consistently indicates the presence of multifractality and the absence of a global scaling regime. This empirical structure is incompatible with the assumption of homogeneous Hölder continuity underlying the rough volatility framework.

The multifractality observed in Bitcoin likely arises from structural features specific to cryptocurrency markets. These include fragmented liquidity, abrupt price movements,

and regime shifts shaped by technological and regulatory developments. Such conditions generate heterogeneous trading behaviour and fluctuating activity levels, which are established drivers of multifractal scaling in financial time series Bacry et al. (2001); Calvet and Fisher (2002). As a result, Bitcoin volatility displays local scaling properties that vary over time and across frequencies, precluding the use of a single global roughness exponent.

This structural heterogeneity explains the empirical failure of roughness estimation techniques in our study. Rather than indicating a methodological flaw, the estimator’s breakdown underscores the fundamental incompatibility between rough volatility assumptions and the multifractal structure of Bitcoin markets.

## 5.2 Implications for Modelling

The structural properties of Bitcoin volatility identified in this study raise concerns about the theoretical validity of applying rough volatility models in this setting. These models rely on the presence of a global scaling regime and homogeneous Hölder continuity. However, empirical findings show that Bitcoin volatility exhibits scale-dependent dynamics and temporal heterogeneity, which violate these fundamental assumptions. Consequently, the existence of a well-defined roughness index cannot be substantiated for Bitcoin.

This incompatibility motivates a broader reconsideration of modelling frameworks for assets that exhibit multifractal characteristics. Models that enforce constant scaling behaviour or a single global regularity parameter are not suitable for processes governed by local, time-varying dynamics. In particular, estimation techniques such as the normalised  $p$ -variation Cont and Das (2024) and log-log regressions Fukasawa et al. (2022); Rogers (2019) lose both interpretability and statistical consistency when applied to processes lacking global scaling symmetry.

In contrast, multifractal modelling frameworks offer a more theoretically coherent basis for capturing the empirical behaviour of Bitcoin volatility Calvet and Fisher (2002); Bacry et al. (2001). Approaches such as the multifractal random walk Bacry et al. (2001) and multifractal stochastic volatility Calvet and Fisher (2002) allow for non-linear scaling and dynamic heterogeneity without requiring a constant roughness parameter. These models are better aligned with the mathematical properties observed in the data and avoid the structural misspecification inherent in rough volatility assumptions Cont and Das (2024).

## 5.3 Practical Consequences

The failure of normalised  $p$ -variation estimation, coupled with the presence of multifractality in Bitcoin volatility, has significant implications for practical applications in forecasting, pricing, and risk management. These findings demonstrate that methods relying on global scaling assumptions are unreliable in the context of cryptocurrency markets.

In practical applications, volatility models used for calibration and prediction must be validated within the specific asset class. In the case of Bitcoin, the absence of a stable roughness index leads to unstable parameter estimates and poor out-of-sample performance when rough volatility models are employed. Volatility models calibrated to equity or foreign exchange markets Gatheral et al. (2018) are not directly transferable to cryptocurrencies, given the structural differences in volatility dynamics.

Reliable volatility forecasting and option pricing for Bitcoin require models that can capture its scale-dependent and time-varying structure. Standard approaches, including GARCH-type models and those assuming constant Hölder regularity, tend to underestimate long memory and tail risk. In contrast, multifractal stochastic volatility models Calvet and Fisher (2002) and wavelet-based methods offer more robust predictive performance by capturing the non-linear and scale-dependent dependencies observed in Bitcoin data.

Practical implementation must also account for market microstructure effects. Bitcoin markets exhibit fragmented liquidity, irregular order flow, and evolving conditions that induce local scaling irregularities and long-range dependence. These features are not captured by standard continuous-path diffusion models. Effective applications such as market-making, hedging, and intraday risk management require models that incorporate structural elements including jumps, regime shifts, and fluctuations in trading activity. Neglecting these factors leads to distorted risk assessments and degraded model performance in high-frequency or volatile environments.

## 5.4 Limitations and Future Work

While this study highlights the limitations of rough volatility estimation for Bitcoin and confirms the presence of multifractal structure, several limitations should be acknowledged. The study focuses exclusively on realised volatility derived from high-frequency price data. Although well-suited for  $p$ -variation analysis, this measure captures only a subset of the latent volatility process. The scaling behaviour of alternative measures, such as implied volatility or state-space estimates, has not been examined. Extending the analysis to these measures would clarify whether multifractality is an intrinsic property of Bitcoin volatility or an artefact of realised volatility estimation, and would offer insights into how market expectations reflect multiscale behaviour.

Second, despite careful preprocessing and partitioning following best practices Cont and Das (2024), our results remain subject to finite-sample limitations. While stationarity and stability diagnostics mitigate concerns about artefactual distortions, the evolving and volatile nature of Bitcoin’s microstructure may still introduce residual biases. Future research could assess the robustness of these findings under alternative sampling schemes, adaptive windowing methods, or extended time horizons (60-day or 120-day windows) to evaluate sensitivity to temporal resolution and aggregation scale.

Third, while our multifractality diagnostics, MF-DFA, log-log scaling, and wavelet leaders, yield consistent results, they are descriptive and empirical. Rigorously confirming multifractal dynamics and distinguishing them from noise or artefacts requires formal statistical testing, including confidence intervals and significance assessments. Approaches such as Wendt et al. (2007) provide a promising foundation. Applying these methods to high-frequency crypto data would constitute a valuable methodological contribution, strengthening the empirical validity of findings in this domain.

These results motivate the development of multifractal or multiscale volatility models tailored to the structural features of Bitcoin markets. Extending the analysis to other crypto-assets such as Ethereum and to traditional markets such as foreign exchange and equities would help determine whether the observed scaling behaviour is specific to Bitcoin or reflects broader properties common to digital assets. Such comparisons would contribute to a more unified understanding of volatility across diverse markets.

## 6 Conclusion

This study assessed the applicability of rough volatility methodologies to Bitcoin using the normalised  $p$ -variation framework proposed by Cont and Das (2024). The statistic  $\log W(L, K, p)$  remains strictly negative across all configurations, precluding the estimation of a valid roughness index. Diagnostic tests rule out non-stationarity, structural breaks, and sampling artefacts as plausible explanations. Instead, consistent evidence from MF-DFA, log-log moment scaling, and wavelet leaders indicates that Bitcoin realised volatility follows a robust multifractal temporal structure, driven by dynamic correlations rather than marginal distributional effects. This violates the homogeneity assumptions required by rough volatility models and accounts for the systematic failure of the estimator.

These findings demonstrate that Bitcoin volatility cannot be adequately described by a single roughness parameter or Hurst exponent. This result is robust across all frequencies, time periods, and estimation settings. Consequently, rough volatility models are structurally incompatible with Bitcoin and are likely to produce unreliable forecasts and pricing outcomes. Models that incorporate multifractal or scale-dependent behaviour, such as multifractal stochastic volatility models, offer a more appropriate empirical fit. Future research should extend this analysis to alternative volatility measures, asset classes, and modelling frameworks to foster a broader understanding of volatility across heterogeneous markets.

# Appendix A: Supplementary Tables

Table A.1: Retained and excluded years by frequency after applying 90% completeness threshold (2017–2024).

Frequency	Years Retained
1-min	2017, 2018, 2019, 2020, 2021, 2022, 2023, 2024
5-min	2017, 2018, 2019, 2020, 2021, 2022, 2023, 2024
10-min	2017, 2018, 2019, 2020, 2021, 2024
15-min	2018, 2019, 2020, 2021, 2024
Frequency	Years Excluded (Below 90%)
1-min	None
5-min	None
10-min	2022, 2023
15-min	2017, 2022, 2023

Table A.2: Summary of missing data and large gaps (>1 hour) by frequency and year in retained 90-day BTC windows.

Frequency	Year	Total Missing Minutes	Gaps >1 Hour (Count)
1-min	2017	1586	0
1-min	2018	420	0
1-min	2019	601	1
1-min	2020	602	0
1-min	2021	136	0
1-min	2022	2016	1
1-min	2023	2918	1
1-min	2024	1097	2
5-min	2017	6275	0
5-min	2018	1885	0
5-min	2019	2490	1
5-min	2020	2705	0
5-min	2021	625	0
5-min	2022	8265	3
5-min	2023	12285	3
5-min	2024	4340	2
10-min	2017	10770	10
10-min	2018	3500	0
10-min	2019	4590	1
10-min	2020	4990	3
10-min	2021	1230	0
10-min	2024	7760	4
15-min	2018	4815	0
15-min	2019	6525	3
15-min	2020	6915	6
15-min	2021	1800	0
15-min	2024	10695	13

Table A.3: ADF Stationarity Summary Table

Frequency	Year	$N_{\text{obs}}$	ADF_stat	$p$ -value	Stationary
1min	2017	128013	-17.268377	$5.88 \times 10^{-30}$	True
1min	2018	129179	-21.103397	0.00	True
1min	2019	128998	-22.996778	0.00	True
1min	2020	128997	-16.217826	$3.93 \times 10^{-29}$	True
1min	2021	129463	-19.473206	0.00	True
1min	2022	127583	-20.992987	0.00	True
1min	2023	126681	-20.199538	0.00	True
1min	2024	128502	-19.502510	0.00	True
5min	2017	24664	-10.745265	$2.75 \times 10^{-19}$	True
5min	2018	25542	-12.375319	$5.17 \times 10^{-23}$	True
5min	2019	25421	-12.273721	$8.53 \times 10^{-23}$	True
5min	2020	25378	-10.130513	$8.94 \times 10^{-18}$	True
5min	2021	25794	-10.793006	$2.11 \times 10^{-19}$	True
5min	2022	24266	-13.884217	$6.13 \times 10^{-26}$	True
5min	2023	23461	-17.513342	$4.32 \times 10^{-30}$	True
5min	2024	25051	-11.923340	$4.97 \times 10^{-22}$	True
10min	2017	11882	-7.661084	$1.69 \times 10^{-11}$	True
10min	2018	12609	-8.932990	$9.70 \times 10^{-15}$	True
10min	2019	12500	-9.974204	$2.20 \times 10^{-17}$	True
10min	2020	12460	-7.922876	$3.68 \times 10^{-12}$	True
10min	2021	12836	-8.282212	$4.49 \times 10^{-13}$	True
10min	2024	12183	-12.177698	$1.37 \times 10^{-22}$	True
15min	2018	8318	-7.222499	$2.09 \times 10^{-10}$	True
15min	2019	8204	-8.225838	$6.25 \times 10^{-13}$	True
15min	2020	8178	-7.227016	$2.04 \times 10^{-10}$	True
15min	2021	8519	-7.315916	$1.23 \times 10^{-10}$	True
15min	2024	7926	-8.943357	$9.13 \times 10^{-15}$	True

Table A.4: Rolling Mean/Variance Stability Table  
(Standard deviation of rolling mean/variance; lower = more stable)

Frequency	Year	$N_{\text{obs}}$	RollingWindow	RollingMeanStd	RollingVarStd
1min	2017	128013	6400	0.000487	$1.69 \times 10^{-6}$
1min	2018	129179	6458	0.000276	$5.53 \times 10^{-7}$
1min	2019	128998	6449	0.000310	$9.69 \times 10^{-7}$
1min	2020	128997	6449	0.000537	$3.24 \times 10^{-6}$
1min	2021	129463	6473	0.000322	$1.00 \times 10^{-6}$
1min	2022	127583	6379	0.000148	$2.63 \times 10^{-7}$
1min	2023	126681	6334	0.000136	$1.93 \times 10^{-7}$
1min	2024	128502	6425	0.000176	$2.61 \times 10^{-7}$
5min	2017	24664	1233	0.001242	$1.00 \times 10^{-5}$
5min	2018	25542	1277	0.000629	$2.72 \times 10^{-6}$
5min	2019	25421	1271	0.000766	$5.94 \times 10^{-6}$
5min	2020	25378	1268	0.001294	$1.85 \times 10^{-5}$
5min	2021	25794	1289	0.000762	$4.88 \times 10^{-6}$
5min	2022	24266	1213	0.000355	$1.48 \times 10^{-6}$
5min	2023	23461	1173	0.000315	$1.12 \times 10^{-6}$
5min	2024	25051	1252	0.000394	$1.23 \times 10^{-6}$
10min	2017	11882	594	0.001835	$2.01 \times 10^{-5}$
10min	2018	12609	630	0.000910	$5.43 \times 10^{-6}$
10min	2019	12500	625	0.001055	$1.71 \times 10^{-5}$
10min	2020	12460	623	0.001861	$3.78 \times 10^{-5}$
10min	2021	12836	641	0.001109	$9.78 \times 10^{-6}$
10min	2024	12183	609	0.000546	$2.65 \times 10^{-6}$
15min	2018	8318	415	0.001161	$8.16 \times 10^{-6}$
15min	2019	8204	410	0.001331	$2.25 \times 10^{-5}$
15min	2020	8178	408	0.002326	$6.73 \times 10^{-5}$
15min	2021	8519	425	0.001435	$1.72 \times 10^{-5}$
15min	2024	7926	396	0.000666	$3.50 \times 10^{-6}$

Table A.5: Structural Breakpoints Detected by Binary Segmentation (Maximum 5 per Series)

Frequency	Year	$N_{\text{obs}}$	#Breaks	Break Indices
1min	2017	128,013	5	[81,225, 93,345, 98,420, 110,855, 118,520]
1min	2018	129,179	5	[20,100, 32,830, 50,455, 64,455, 69,100]
1min	2019	128,998	5	[10,335, 60,520, 66,495, 77,840, 100,395]
1min	2020	128,997	5	[100,870, 101,400, 101,440, 103,445, 118,760]
1min	2021	129,463	5	[2,475, 14,290, 18,080, 42,755, 92,420]
1min	2022	127,583	5	[25,405, 34,420, 70,240, 75,450, 103,895]
1min	2023	126,681	5	[5,480, 26,570, 76,555, 85,755, 107,190]
1min	2024	128,502	5	[51,000, 75,290, 87,365, 118,305, 118,780]
5min	2017	24,664	5	[15,335, 17,530, 18,760, 21,230, 22,790]
5min	2018	25,542	5	[3,960, 6,475, 6,495, 9,870, 14,860]
5min	2019	25,421	5	[2,060, 11,985, 13,180, 15,440, 19,885]
5min	2020	25,378	5	[19,980, 20,085, 20,090, 20,535, 23,675]
5min	2021	25,794	5	[495, 2,855, 3,605, 8,195, 8,490]
5min	2022	24,266	5	[4,760, 6,785, 13,240, 14,580, 19,765]
5min	2023	23,461	5	[995, 4,715, 15,780, 18,055, 19,885]
5min	2024	25,051	5	[9,810, 14,640, 17,065, 23,055, 23,145]
10min	2017	11,882	5	[7,220, 7,495, 10,165, 10,480, 10,945]
10min	2018	12,609	5	[2,060, 3,185, 3,195, 4,890, 7,305]
10min	2019	12,500	5	[890, 900, 1,030, 5,925, 9,840]
10min	2020	12,460	5	[9,875, 10,000, 10,035, 10,155, 11,645]
10min	2021	12,836	5	[245, 1,430, 1,600, 1,830, 4,240]
10min	2024	12,183	5	[4,700, 7,105, 8,300, 11,205, 11,255]
15min	2018	8,318	5	[1,305, 2,095, 2,105, 3,185, 4,800]
15min	2019	8,204	5	[680, 3,905, 4,305, 4,965, 6,505]
15min	2020	8,178	5	[6,550, 6,600, 6,620, 6,675, 7,565]
15min	2021	8,519	5	[160, 950, 1,065, 1,205, 2,825]
15min	2024	7,926	5	[3,010, 3,905, 4,610, 5,380, 7,195]

Table A.6: Summary of MF-DFA Scaling Exponents  $H(q)$  for Bitcoin Log>Returns (Original vs. Shuffled, 2017–2024). Table reports minimum, maximum, mean, and width (max – min) of  $H(q)$  spectra.

Freq.	Year	Original $H(q)$				Shuffled $H(q)$			
		Min	Max	Mean	Width	Min	Max	Mean	Width
1min	2017	0.404	2.167	1.148	1.763	0.468	0.530	0.501	0.061
1min	2018	0.442	0.610	0.528	0.168	0.472	0.540	0.509	0.068
1min	2019	0.356	0.595	0.515	0.239	0.417	0.539	0.504	0.122
1min	2020	0.368	0.572	0.517	0.204	0.418	0.540	0.507	0.122
1min	2021	0.410	0.556	0.503	0.146	0.470	0.540	0.510	0.070
1min	2022	0.443	0.587	0.524	0.144	0.460	0.541	0.508	0.081
1min	2023	0.448	0.562	0.515	0.114	0.463	0.570	0.515	0.107
1min	2024	0.419	0.616	0.523	0.197	0.444	0.521	0.490	0.077
5min	2017	0.392	0.614	0.509	0.222	0.502	0.593	0.540	0.091
5min	2018	0.425	0.608	0.527	0.183	0.480	0.546	0.518	0.066
5min	2019	0.345	0.617	0.511	0.272	0.463	0.586	0.529	0.123
5min	2020	0.332	0.592	0.498	0.260	0.439	0.635	0.547	0.196
5min	2021	0.405	0.571	0.510	0.166	0.463	0.557	0.515	0.094
5min	2022	0.453	0.585	0.527	0.132	0.458	0.549	0.515	0.091
5min	2023	0.455	0.730	0.555	0.275	0.436	0.563	0.499	0.127
5min	2024	0.412	0.642	0.525	0.230	0.453	0.549	0.507	0.096
10min	2017	0.379	0.617	0.522	0.237	0.526	0.610	0.564	0.084
10min	2018	0.422	0.622	0.533	0.200	0.497	0.593	0.545	0.096
10min	2019	0.339	0.635	0.520	0.296	0.397	0.594	0.526	0.197
10min	2020	0.365	0.611	0.512	0.246	0.402	0.636	0.539	0.234
10min	2021	0.403	0.579	0.515	0.176	0.446	0.530	0.499	0.084
10min	2024	0.400	0.662	0.527	0.262	0.473	0.592	0.537	0.119
15min	2018	0.429	0.637	0.533	0.208	0.506	0.601	0.552	0.095
15min	2019	0.365	0.645	0.523	0.281	0.448	0.625	0.545	0.177
15min	2020	0.342	0.630	0.506	0.288	0.370	0.653	0.540	0.283
15min	2021	0.394	0.586	0.511	0.192	0.466	0.555	0.513	0.089
15min	2024	0.402	0.653	0.527	0.251	0.452	0.564	0.512	0.112

Table A.7: Summary of Log-Log Scaling Exponents for Bitcoin Log>Returns (Original vs. Shuffled, 2017–2024). Table reports minimum, maximum, mean, and width (max – min) of scaling coefficients.

Freq.	Year	Original				Shuffled			
		Min	Max	Mean	Width	Min	Max	Mean	Width
1min	2017	-4.919	0.005	-0.963	4.924	0.000	0.337	0.102	0.337
1min	2018	-3.914	0.003	-0.796	3.917	0.000	0.500	0.150	0.500
1min	2019	-2.798	0.004	-0.564	2.802	0.000	0.343	0.086	0.343
1min	2020	-2.964	0.007	-0.555	2.971	-0.001	0.554	0.108	0.555
1min	2021	-0.064	1.407	0.229	1.471	-0.036	0.000	-0.108	0.036
1min	2022	-2.379	0.005	-0.654	2.384	0.000	0.593	0.117	0.593
1min	2023	-0.034	0.009	-0.235	0.043	0.000	0.177	0.042	0.177
1min	2024	-1.420	0.007	-0.408	1.427	-0.001	0.083	0.016	0.083
5min	2017	-1.812	0.007	-0.494	1.819	-0.001	0.959	0.235	0.960
5min	2018	-0.014	0.003	-0.123	0.017	-0.005	0.242	0.047	0.247
5min	2019	-0.105	0.533	0.130	0.638	-0.002	0.000	-0.073	0.002
5min	2020	-2.053	0.009	-0.487	2.062	-0.000	1.004	0.293	1.004
5min	2021	-0.058	0.007	-0.103	0.065	-0.002	0.065	0.021	0.067
5min	2022	-0.023	0.005	-0.106	0.028	0.000	0.999	0.094	0.999
5min	2023	-0.021	0.009	-0.338	0.030	-0.001	0.010	0.003	0.010
5min	2024	-0.041	0.007	-0.406	0.048	-0.010	-0.312	-0.063	0.302
10min	2017	-0.084	0.068	0.008	0.152	-0.949	0.000	-0.333	0.949
10min	2018	-0.016	0.135	0.029	0.151	-0.115	0.000	-0.045	0.115
10min	2019	-0.360	0.002	-0.079	0.362	-0.168	0.001	-0.048	0.168
10min	2020	-1.166	0.008	-0.333	1.174	-0.345	0.007	-0.078	0.352
10min	2021	-1.341	0.004	-0.303	1.345	-0.688	0.005	-0.102	0.693
10min	2024	-1.239	0.006	-0.304	1.245	-0.007	0.197	0.031	0.204
15min	2018	-1.732	0.001	-0.391	1.733	-0.205	0.004	-0.036	0.209
15min	2019	-0.019	0.001	-0.107	0.021	-0.633	0.029	-0.129	0.662
15min	2020	-0.127	1.682	0.284	1.809	0.000	0.495	0.151	0.495
15min	2021	-0.087	0.006	-0.119	0.093	-0.009	0.124	0.029	0.133
15min	2024	-0.062	0.006	-0.225	0.068	-0.009	0.262	0.035	0.271

Table A.8: Summary of Wavelet Leaders Scaling Exponents for Bitcoin Log>Returns (Original vs. Shuffled, 2017–2024). Table reports minimum, maximum, mean, and width (max – min) for each case.

Freq.	Year	Original				Shuffled			
		Min	Max	Mean	Width	Min	Max	Mean	Width
1min	2017	-0.200	0.063	-0.036	0.263	-0.167	-0.001	-0.119	0.166
1min	2018	-0.190	0.060	-0.024	0.250	-0.146	-0.054	-0.110	0.092
1min	2019	-0.245	0.047	-0.078	0.292	-0.152	-0.069	-0.098	0.083
1min	2020	-0.249	0.124	-0.034	0.373	-0.144	-0.046	-0.096	0.098
1min	2021	-0.199	0.140	-0.096	0.339	-0.122	-0.008	-0.056	0.114
1min	2022	-0.195	-0.015	-0.094	0.180	-0.094	-0.003	-0.037	0.091
1min	2023	-0.123	0.146	0.017	0.269	-0.157	-0.071	-0.110	0.086
1min	2024	-0.199	0.043	-0.057	0.242	-0.164	-0.050	-0.094	0.114
5min	2017	-0.217	0.079	-0.039	0.297	-0.218	-0.008	-0.154	0.210
5min	2018	-0.220	0.002	-0.069	0.222	-0.044	0.016	-0.008	0.060
5min	2019	-0.252	0.073	-0.043	0.325	-0.206	-0.103	-0.143	0.103
5min	2020	-0.236	0.137	-0.010	0.372	-0.316	-0.001	-0.116	0.315
5min	2021	-0.181	-0.060	-0.107	0.121	-0.199	-0.082	-0.120	0.117
5min	2022	-0.114	0.039	-0.032	0.153	-0.146	-0.031	-0.086	0.115
5min	2023	-0.118	0.061	0.004	0.179	-0.196	-0.149	-0.159	0.047
5min	2024	-0.115	0.105	0.016	0.220	-0.249	-0.007	-0.158	0.242
10min	2017	-0.015	0.189	0.074	0.204	-0.060	0.042	0.000	0.102
10min	2018	-0.215	0.009	-0.088	0.225	-0.185	0.001	-0.067	0.186
10min	2019	-0.143	0.124	-0.018	0.267	-0.174	0.118	-0.020	0.292
10min	2020	-0.039	0.165	0.046	0.204	-0.249	0.127	-0.037	0.377
10min	2021	-0.188	-0.040	-0.104	0.148	-0.114	-0.023	-0.058	0.091
10min	2024	-0.268	0.093	-0.050	0.362	-0.019	0.185	0.061	0.204
15min	2018	-0.194	-0.021	-0.082	0.173	-0.008	0.113	0.040	0.121
15min	2019	-0.228	0.059	-0.066	0.288	-0.383	-0.037	-0.176	0.346
15min	2020	-0.037	0.190	0.049	0.227	-0.160	0.130	-0.012	0.290
15min	2021	-0.159	-0.067	-0.109	0.092	-0.199	-0.003	-0.087	0.197
15min	2024	-0.220	0.081	-0.037	0.301	-0.009	0.041	0.018	0.050

Table A.9: Summary of MF-DFA Scaling Exponents  $H(q)$  for Bitcoin Realised Volatility (Original vs. Shuffled, 2017–2024). Table reports minimum, maximum, mean, and width (max – min) of  $H(q)$  spectra.

Freq.	Year	Original $H(q)$				Shuffled $H(q)$			
		Min	Max	Mean	Width	Min	Max	Mean	Width
1min	2017	0.863	2.082	1.351	1.219	0.460	0.550	0.504	0.090
1min	2018	0.812	0.867	0.848	0.055	0.487	0.572	0.531	0.085
1min	2019	0.748	0.912	0.876	0.163	0.395	0.558	0.510	0.163
1min	2020	0.871	0.945	0.896	0.074	0.422	0.618	0.534	0.195
1min	2021	0.829	0.920	0.894	0.091	0.457	0.559	0.517	0.102
1min	2022	0.781	0.939	0.872	0.158	0.453	0.579	0.526	0.126
1min	2023	0.780	0.931	0.867	0.151	0.438	0.581	0.518	0.143
1min	2024	0.814	1.023	0.921	0.209	0.462	0.572	0.527	0.110
5min	2017	0.850	0.918	0.901	0.068	0.470	0.591	0.533	0.121
5min	2018	0.779	0.904	0.854	0.125	0.460	0.594	0.530	0.134
5min	2019	0.642	0.948	0.837	0.306	0.411	0.612	0.527	0.200
5min	2020	0.814	0.942	0.885	0.128	0.425	0.676	0.549	0.251
5min	2021	0.820	0.907	0.886	0.087	0.439	0.578	0.517	0.139
5min	2022	0.726	0.918	0.822	0.192	0.410	0.582	0.526	0.172
5min	2023	0.730	1.040	0.871	0.310	0.428	0.595	0.523	0.167
5min	2024	0.791	0.969	0.876	0.178	0.393	0.563	0.508	0.170
10min	2017	0.840	0.946	0.914	0.106	0.494	0.574	0.535	0.080
10min	2018	0.726	0.889	0.834	0.163	0.457	0.593	0.527	0.135
10min	2019	0.592	0.917	0.835	0.324	0.321	0.627	0.526	0.306
10min	2020	0.824	0.863	0.870	0.040	0.352	0.717	0.536	0.365
10min	2021	0.777	0.882	0.862	0.104	0.440	0.586	0.526	0.146
10min	2024	0.767	0.951	0.880	0.184	0.419	0.607	0.516	0.188
15min	2018	0.755	0.912	0.837	0.157	0.475	0.632	0.528	0.157
15min	2019	0.646	0.948	0.834	0.302	0.383	0.667	0.523	0.284
15min	2020	0.758	0.840	0.820	0.082	0.322	0.744	0.527	0.422
15min	2021	0.755	0.874	0.842	0.119	0.419	0.612	0.527	0.193
15min	2024	0.747	0.942	0.870	0.195	0.478	0.654	0.527	0.176

Table A.10: Summary of Log-Log Scaling Exponents for Bitcoin Realised Volatility (Original vs. Shuffled, 2017–2024). Table reports minimum, maximum, mean, and width (max – min) of scaling coefficients.

Freq.	Year	Original				Shuffled			
		Min	Max	Mean	Width	Min	Max	Mean	Width
1min	2017	-5.001	0.066	-0.927	5.067	-0.001	0.338	0.094	0.339
1min	2018	-4.314	0.049	-0.849	4.363	-0.002	1.272	0.328	1.274
1min	2019	-3.714	0.082	-0.754	3.796	-0.002	0.000	-0.096	0.002
1min	2020	-2.628	0.122	-0.451	2.750	-0.000	0.290	0.073	0.290
1min	2021	0.107	1.084	0.446	0.976	-0.008	0.465	0.116	0.473
1min	2022	-2.086	0.054	-0.557	2.140	-0.001	0.569	0.113	0.570
1min	2023	-0.655	0.064	-0.156	0.719	-0.000	0.306	0.055	0.306
1min	2024	-0.933	0.110	-0.208	1.043	-0.001	0.014	0.002	0.015
5min	2017	-3.164	0.101	-0.629	3.265	-0.000	1.204	0.339	1.204
5min	2018	-0.279	0.057	-0.063	0.336	-0.010	-0.000	-0.071	0.010
5min	2019	-0.014	1.010	0.281	1.025	-0.015	0.125	0.026	0.140
5min	2020	-1.702	0.181	-0.283	1.883	0.000	0.411	0.091	0.411
5min	2021	-0.336	0.110	-0.011	0.446	-0.007	0.176	0.022	0.183
5min	2022	-0.359	0.041	-0.059	0.400	0.000	0.220	0.060	0.220
5min	2023	-1.919	0.066	-0.311	1.985	-0.001	0.367	0.068	0.368
5min	2024	-1.503	0.079	-0.202	1.582	-0.007	-0.000	-0.130	0.007
10min	2017	-0.006	0.131	0.045	0.137	-0.793	0.000	-0.195	0.793
10min	2018	-0.121	0.049	-0.022	0.170	-0.561	0.000	-0.130	0.561
10min	2019	-0.024	0.063	0.018	0.087	0.000	0.500	0.133	0.500
10min	2020	-0.548	0.126	-0.067	0.674	-0.328	0.003	-0.061	0.331
10min	2021	-1.739	0.095	-0.354	1.835	-0.163	0.009	-0.018	0.172
10min	2024	-1.962	0.074	-0.281	2.036	-0.000	0.168	0.042	0.168
15min	2018	-1.505	0.035	-0.305	1.540	-0.002	0.041	0.013	0.043
15min	2019	-0.004	0.590	0.142	0.594	-1.786	0.010	-0.377	1.796
15min	2020	-0.010	0.996	0.317	1.006	0.000	0.236	0.067	0.236
15min	2021	-0.006	0.286	0.094	0.292	0.000	0.145	0.025	0.145
15min	2024	-1.249	0.091	-0.193	1.340	-0.002	0.152	0.038	0.154

Table A.11: Summary of Wavelet Leaders Scaling Exponents for Bitcoin Realised Volatility (Original vs. Shuffled, 2017–2024). Table reports minimum, maximum, mean, and width (max – min) for each case.

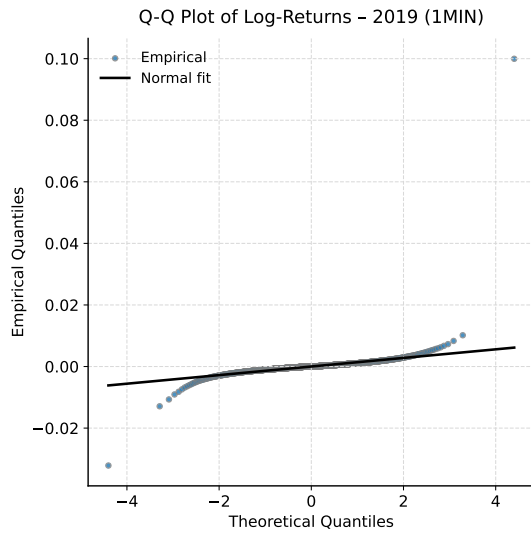
Freq.	Year	Original				Shuffled			
		Min	Max	Mean	Width	Min	Max	Mean	Width
1min	2017	-0.676	-0.310	-0.420	0.367	-0.205	-0.092	-0.121	0.113
1min	2018	-0.512	-0.269	-0.358	0.243	-0.171	-0.086	-0.109	0.085
1min	2019	-0.453	-0.218	-0.324	0.235	-0.128	0.025	-0.049	0.153
1min	2020	-0.493	-0.311	-0.384	0.182	-0.230	-0.010	-0.101	0.220
1min	2021	-0.435	-0.292	-0.356	0.143	-0.164	-0.006	-0.068	0.158
1min	2022	-0.428	-0.244	-0.328	0.184	-0.175	-0.079	-0.106	0.096
1min	2023	-0.596	-0.245	-0.382	0.351	-0.173	-0.025	-0.079	0.148
1min	2024	-0.512	-0.277	-0.385	0.235	-0.149	0.060	-0.019	0.209
5min	2017	-0.452	-0.278	-0.363	0.174	-0.271	-0.172	-0.197	0.099
5min	2018	-0.359	-0.187	-0.277	0.172	-0.236	-0.010	-0.088	0.227
5min	2019	-0.531	-0.187	-0.347	0.344	-0.226	0.070	-0.043	0.296
5min	2020	-0.296	-0.255	-0.319	0.041	-0.304	0.063	-0.059	0.367
5min	2021	-0.309	-0.275	-0.308	0.034	0.039	0.096	0.061	0.057
5min	2022	-0.191	-0.039	-0.107	0.151	-0.197	-0.075	-0.119	0.122
5min	2023	-0.421	-0.208	-0.312	0.213	-0.148	-0.025	-0.069	0.123
5min	2024	-0.513	-0.219	-0.352	0.294	-0.177	-0.066	-0.121	0.111
10min	2017	-0.323	-0.167	-0.270	0.156	-0.159	0.008	-0.055	0.167
10min	2018	-0.482	-0.165	-0.306	0.318	-0.257	-0.002	-0.133	0.255
10min	2019	-0.393	-0.156	-0.289	0.237	-0.249	0.066	-0.066	0.315
10min	2020	-0.199	-0.215	-0.256	0.016	-0.241	0.118	-0.034	0.359
10min	2021	-0.354	-0.254	-0.309	0.100	-0.166	-0.045	-0.086	0.121
10min	2024	-0.522	-0.243	-0.378	0.279	-0.245	-0.012	-0.082	0.233
15min	2018	-0.371	-0.154	-0.263	0.217	-0.158	0.014	-0.058	0.172
15min	2019	-0.463	-0.105	-0.267	0.358	-0.299	0.051	-0.075	0.350
15min	2020	-0.331	-0.211	-0.275	0.120	-0.319	0.194	-0.014	0.513
15min	2021	-0.313	-0.240	-0.282	0.073	-0.215	0.113	-0.017	0.328
15min	2024	-0.583	-0.212	-0.380	0.371	-0.264	-0.032	-0.117	0.232

Table A.12: Minimum and maximum values of  $\log W(L, K, p)$  for each (frequency, year) pair, using the noise-robust realised volatility  $\widetilde{RV}_t^\Delta$ .

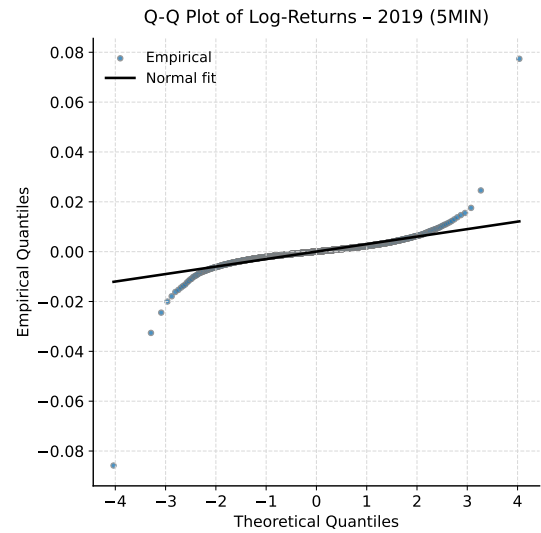
Frequency	Year	Standard Grid		Wide Grid	
		Min	Max	Min	Max
1min	2017	-1.797	-0.090	-1.797	-0.009
1min	2018	-3.454	-0.110	-3.454	-0.011
1min	2019	-3.149	-0.114	-3.149	-0.011
1min	2020	-1.857	-0.124	-1.857	-0.012
1min	2021	-2.377	-0.098	-2.377	-0.010
1min	2022	-5.021	-0.154	-5.021	-0.015
1min	2023	-6.177	-0.199	-6.177	-0.020
1min	2024	-5.249	-0.175	-5.249	-0.018
5min	2017	-1.188	-0.067	-1.188	-0.007
5min	2018	-2.738	-0.089	-2.738	-0.009
5min	2019	-2.625	-0.093	-2.625	-0.009
5min	2020	-1.434	-0.104	-1.434	-0.010
5min	2021	-1.855	-0.079	-1.855	-0.008
5min	2022	-4.442	-0.133	-4.442	-0.013
5min	2023	-5.658	-0.176	-5.658	-0.018
5min	2024	-4.778	-0.155	-4.778	-0.016
10min	2017	-1.093	-0.062	-1.093	-0.006
10min	2018	-2.628	-0.084	-2.628	-0.008
10min	2019	-2.542	-0.089	-2.542	-0.009
10min	2020	-1.388	-0.100	-1.388	-0.010
10min	2021	-1.782	-0.075	-1.782	-0.008
10min	2024	-4.831	-0.150	-4.831	-0.015
15min	2018	-2.588	-0.083	-2.588	-0.008
15min	2019	-2.446	-0.087	-2.446	-0.009
15min	2020	-1.402	-0.099	-1.402	-0.010
15min	2021	-1.908	-0.073	-1.908	-0.007
15min	2024	-4.807	-0.150	-4.807	-0.015

## Appendix B: Supplementary Figures

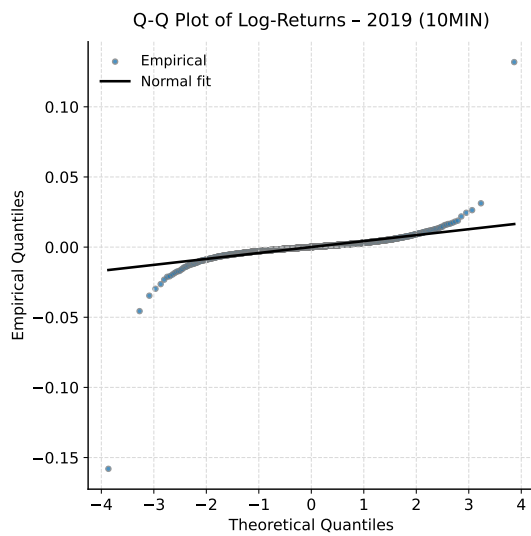
Figure B.1: Quantile–Quantile plots of Bitcoin log-returns in 2019 at multiple sampling frequencies (1-minute, 5-minute, 10-minute, and 15-minute)



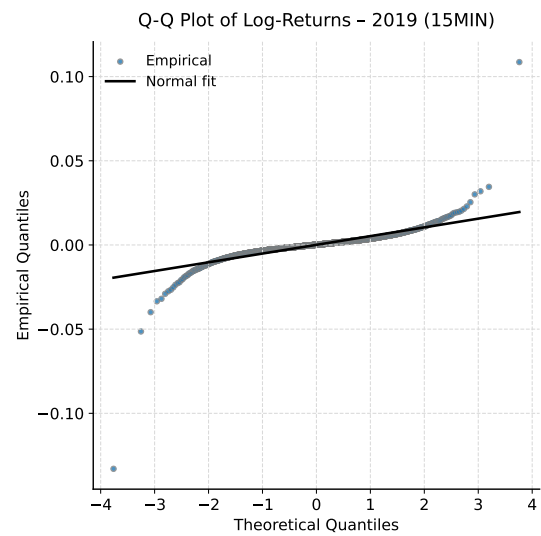
(a) 1-minute



(b) 5-minute

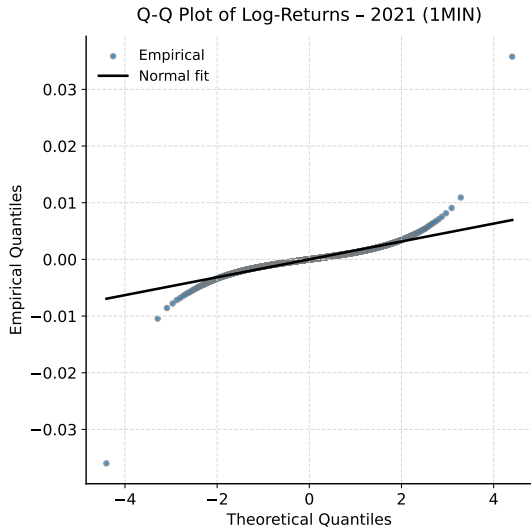


(c) 10-minute

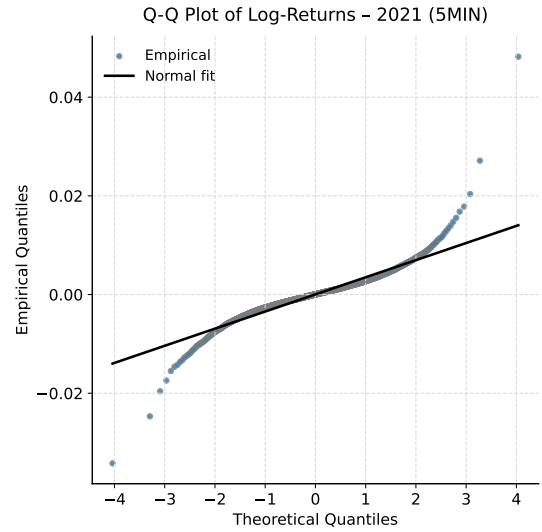


(d) 15-minute

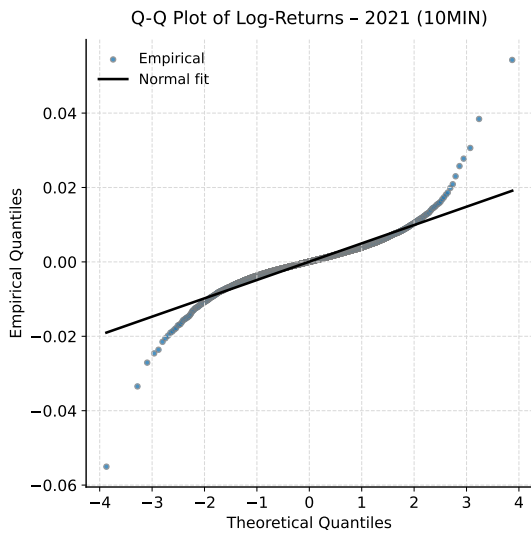
Figure B.2: Quantile–Quantile plots of Bitcoin log-returns in 2021 at multiple sampling frequencies (1-minute, 5-minute, 10-minute, and 15-minute



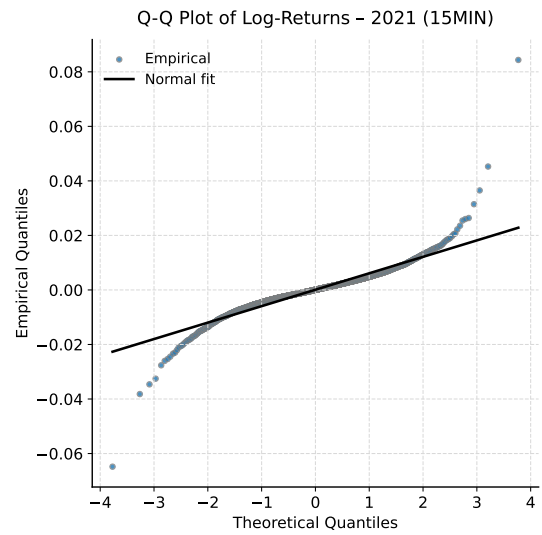
(a) 1-minute



(b) 5-minute

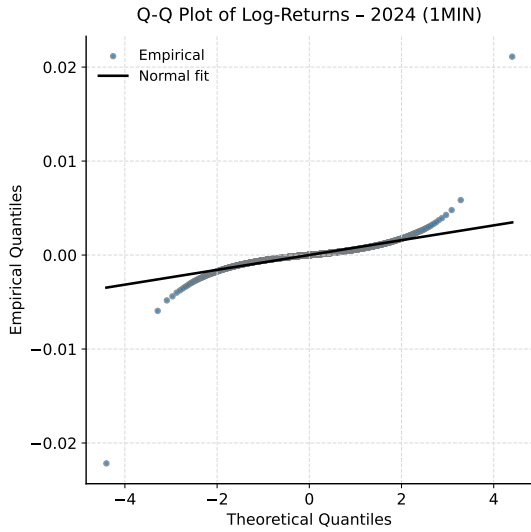


(c) 10-minute

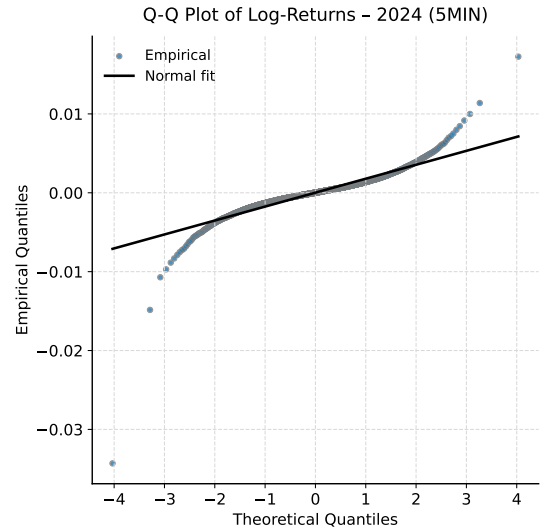


(d) 15-minute

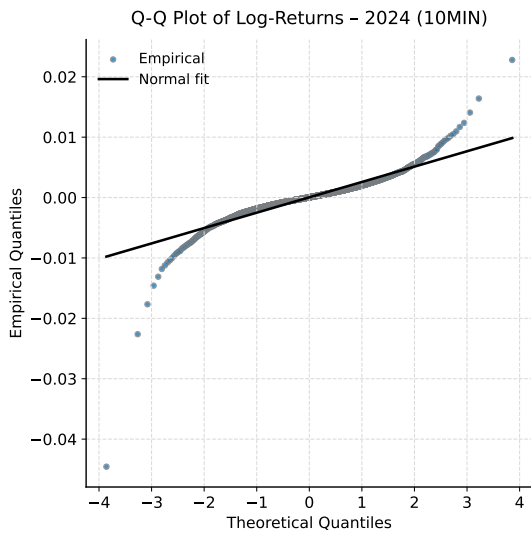
Figure B.3: Quantile–Quantile plots of Bitcoin log-returns in 2024 at multiple sampling frequencies (1-minute, 5-minute, 10-minute, and 15-minute)



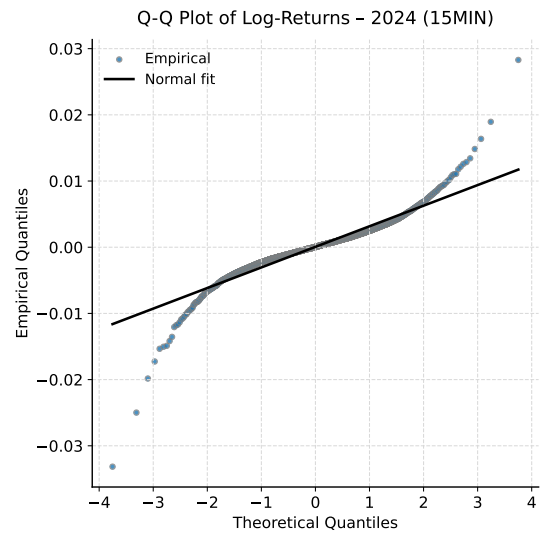
(a) 1-minute



(b) 5-minute

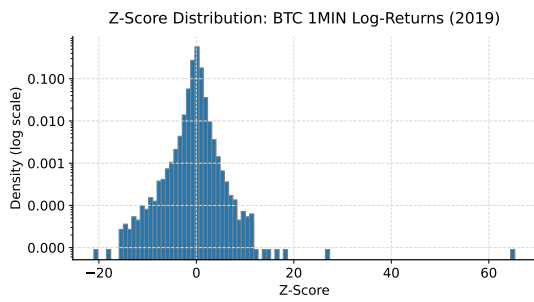


(c) 10-minute

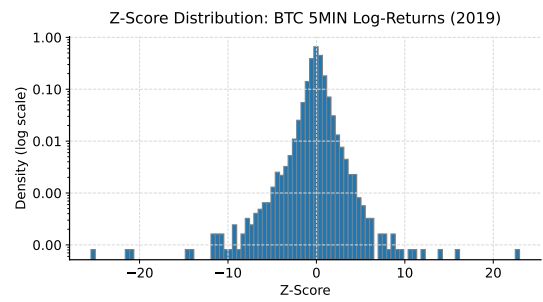


(d) 15-minute

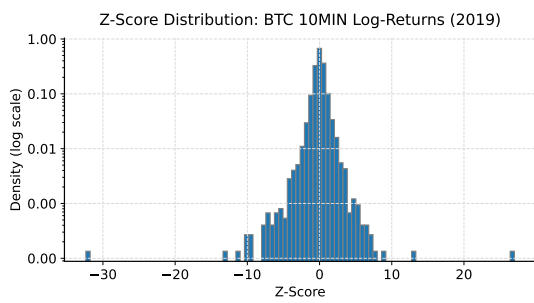
Figure B.4: Z-score histograms of Bitcoin log-returns in 2019 at multiple sampling frequencies (1-minute, 5-minute, 10-minute, and 15-minute), with densities plotted on a logarithmic scale to visualise tail behaviour



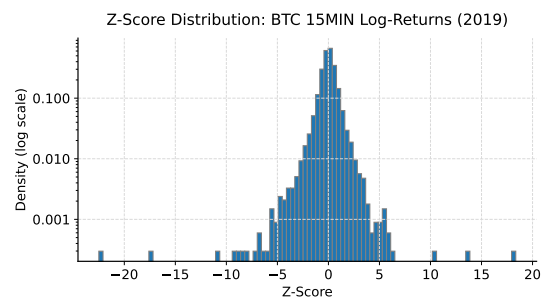
(a) 1-minute



(b) 5-minute

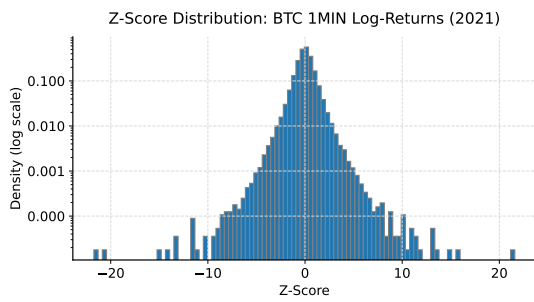


(c) 10-minute

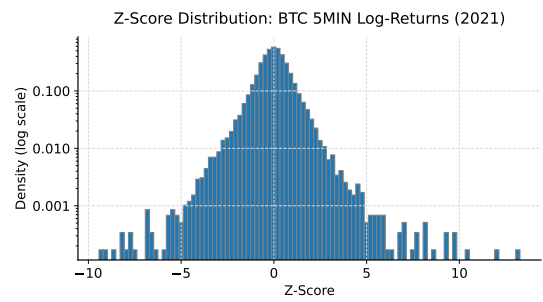


(d) 15-minute

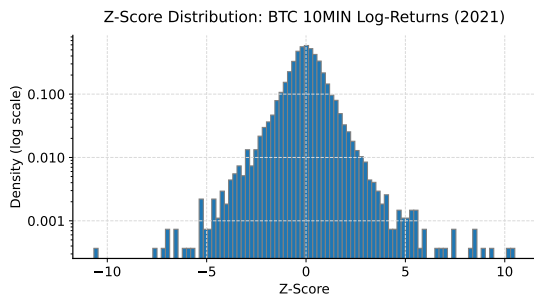
Figure B.5: Z-score histograms of Bitcoin log-returns in 2021 at multiple sampling frequencies (1-minute, 5-minute, 10-minute, and 15-minute), with densities plotted on a logarithmic scale to visualise tail behaviour



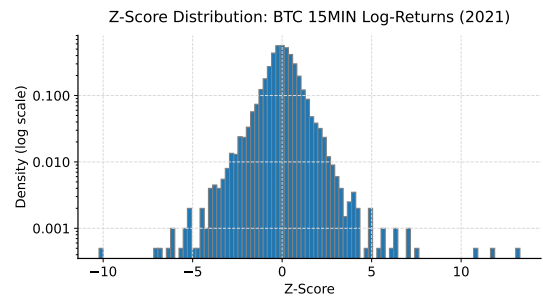
(a) 1-minute



(b) 5-minute

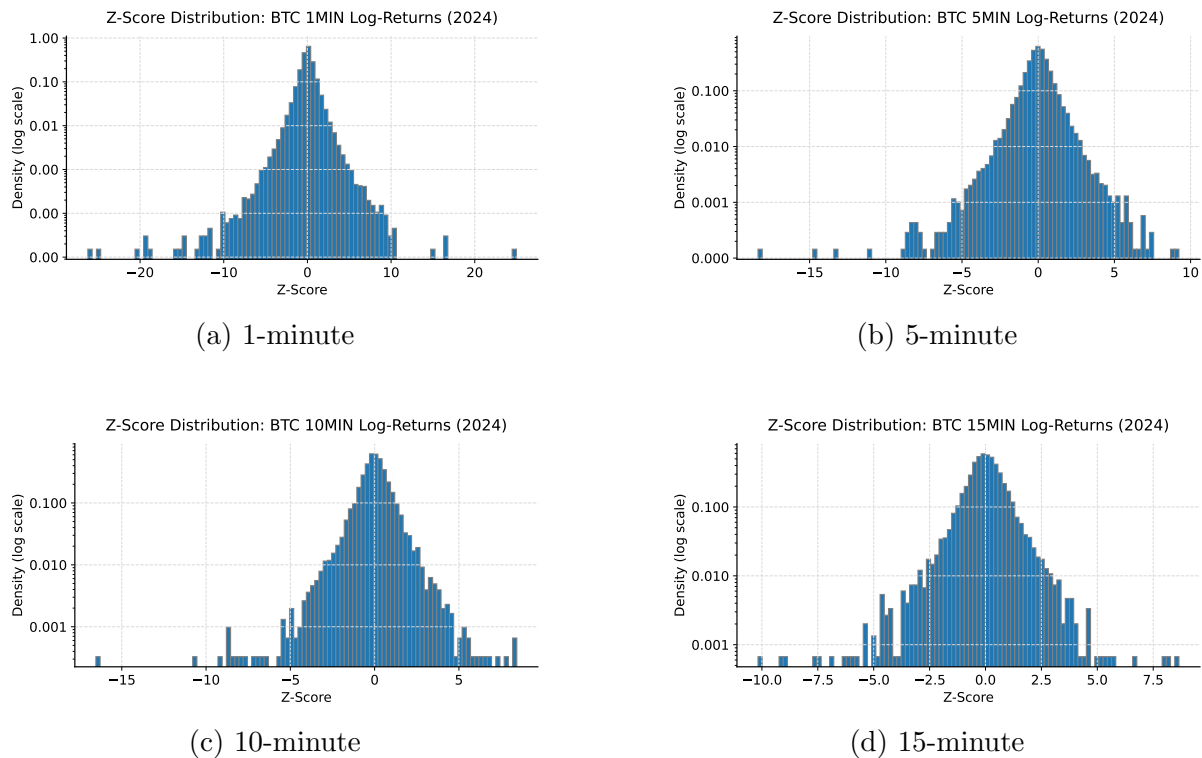


(c) 10-minute



(d) 15-minute

Figure B.6: Z-score histograms of Bitcoin log-returns in 2024 at multiple sampling frequencies (1-minute, 5-minute, 10-minute, and 15-minute), with densities plotted on a logarithmic scale to visualise tail behaviour



## Appendix C: Code and Data Availability

All code used for data processing, analysis, and figure generation is available from the authors upon request. The Bitcoin high-frequency price data are publicly accessible from Kaggle at <https://www.kaggle.com/datasets/mczielinski/bitcoin-historical-data>.

## References

- Bacry, E., Delour, J., and Muzy, J. F. (2001). Multifractal random walk. *Physical Review E*, 64(2):026103.
- Bennedsen, M., Lunde, A., and Pakkanen, M. S. (2016). Decoupling the short- and long-term behavior of stochastic volatility. *Journal of Financial Economics*, 122(3):1–20.
- Bianchi, D. et al. (2022). Cryptocurrency market structure: Stylized facts, scaling laws, and rough volatility. Available at SSRN 4062712.
- Calvet, L. E. and Fisher, A. J. (2002). Multifractality in asset returns: Theory and evidence. *Review of Economics and Statistics*, 84(3):381–406.
- Caporale, G. M. and Zekokh, T. (2021). Regime-switching volatility in cryptocurrency markets. *Research in International Business and Finance*, 55:101303.

- Cont, R. and Das, P. (2024). Rough volatility: Fact or artefact? *Sankhyā B: The Indian Journal of Statistics*.
- Easley, D., O'Hara, M., and Basu, S. (2019). From mining to markets: The evolution of bitcoin transaction fees. *Journal of Financial Economics*, 134(1):91–109.
- Fukasawa, M., Takabatake, T., and Westphal, R. (2022). Consistent estimation for fractional stochastic volatility model under high-frequency asymptotics. *Mathematical Finance*, 32(4):1086–1132.
- Gatheral, J., Jaisson, T., and Rosenbaum, M. (2018). Volatility is rough. *Quantitative Finance*, 18(6):933–949.
- Kantelhardt, J. W., Zschiegner, S. A., Koscielny-Bunde, E., Havlin, S., Bunde, A., and Stanley, H. E. (2002). Multifractal detrended fluctuation analysis of nonstationary time series. *Physica A: Statistical Mechanics and its Applications*, 316(1–4):87–114.
- Lahmiri, S. and Bekiros, S. (2020). Chaos, randomness and multi-fractality in bitcoin market. *Chaos, Solitons & Fractals*, 133:109641.
- Liu, Y. and Tsyvinski, A. (2021). Risks and returns of cryptocurrency. *The Review of Financial Studies*, 34(6):2689–2727.
- Makarov, I. and Schoar, A. (2020). Trading and arbitrage in cryptocurrency markets. *Journal of Financial Economics*, 135(2):293–319.
- Matteo, T. D. (2007). Multi-scaling in finance. *Quantitative Finance*, 7(1):21–36.
- Mensi, W., Vo, X. V., Hammoudeh, S., and Vo, D. H. (2019). Multifractality and return predictability in the cryptocurrency market: Evidence from bitcoin, ethereum, and ripple. *Chaos, Solitons & Fractals*, 132:109924.
- Rogers, L. C. G. (2019). Things we think we know. Available at <https://www.skokholm.co.uk/wp-content/uploads/2019/11/TWTWKpaper.pdf>.
- Watorek, M., Kwapien, J., Drożdż, S., Oświecimka, P., and Gubiec, T. (2022). Multi-scale multifractality and cross-correlations in the cryptocurrency market. *Chaos: An Interdisciplinary Journal of Nonlinear Science*, 32(4):043110.
- Wendt, H., Abry, P., and Jaffard, S. (2007). Bootstrap for empirical multifractal analysis. *IEEE Signal Processing Magazine*, 24(4):38–48.
- Zhou, W.-X., Jiang, Z.-Q., and Wang, Q. (2022). Multifractal nature of bitcoin volatility. *Physica A: Statistical Mechanics and its Applications*, 603:127774.